THESIS

# ESTIMATING CHANGES IN STREAMFLOW ATTRIBUTABLE TO WILDFIRE IN MULTIPLE WATERSHEDS USING A SEMI-DISTRIBUTED WATERSHED MODEL

Submitted by

Ryan Wells

Department of Civil and Environmental Engineering

In partial fulfillment of the requirements

For the Degree of Master of Science

Colorado State University

Fort Collins, Colorado

Fall 2023

Master's Committee:

Advisor: Jeffrey D. Niemann

Stephanie Kampf
Peter Nelson

# ABSTRACT

## ESTIMATING CHANGES IN STREAMFLOW ATTRIBUTABLE TO WILDFIRE IN MULTIPLE WATERSHEDS USING A SEMI-DISTRIBUTED WATERSHED MODEL

Over half of western U.S. water supply is sourced from forested lands that are increasingly under wildfire risk. Studies have begun to isolate the effects of wildfire on streamflow, but they have used coarse temporal resolutions that cannot account for the numerous, interconnected watershed processes that control the responses to rainfall events. To address these concerns, we developed a method to isolate fine-scale (daily) effects of fire from climate. Wildfire effects were represented by the difference between measured post-fire daily streamflow and simulated unburned post-fire daily streamflow from a hydrologic model calibrated to pre-fire conditions. The method was applied to track hydrologic recovery after wildfires in six burned watersheds across the western U.S.: North Eagle Creek, NM (2012 Little Bear Fire), Lopez Creek, CA (1985 Las Pilitas Fire), and City Creek, Devil Canyon Creek, East Twin Creek, and Plunge Creek, CA (2003 Old Fire). All six watersheds experienced prolonged increases of post-fire streamflow, with the most consistent changes occurring during periods of low streamflow. Following 6 years of increased streamflow, Lopez Creek experienced 6 years of reduced streamflow, before returning to pre-fire streamflow behavior 12 years after the fire. North Eagle Creek and the four watersheds affected by the Old Fire continued to demonstrate elevated streamflow 9 and 18 years post-fire, respectively. This study demonstrates the utility of examining post-fire streamflow at daily resolution over multiple years. In particular, these results captured the variability of change across flow frequencies during recovery periods that would not be quantifiable otherwise.

ACKNOWLEDGEMENTS

I would first like to thank my thesis advisor, Jeffrey Niemann, for allowing me to join his lab group as a transfer student, helping me to better define my research objectives, and guiding me throughout the final half of my time spent at Colorado State University. Additionally, I would also like to thank everyone in the Ages modeling group at the U.S. Department of Agriculture, particularly the guidance and support received from Kyle Mankin, Tim Green, and Holm Kipka. I would also like to acknowledge Stephanie Kampf and Peter Nelson for participating on my committee and providing additional perspective on this research. Finally, the journey of returning to school was made much easier by the unwavering support and emphasis on the value of education I received from my family, especially my parents and grandparents.

TABLE OF CONTENTS

LIST OF TABLES

LIST OF FIGURES

# 1. INTRODUCTION

Concerns about the impact of wildfires on water supplies are growing as wildfires become larger and more common throughout the American West (Williams et al., 2019a, Abatzoglou et al., 2021, Barnard et al., 2023). Although fire has always played a role in ecosystem health in this region, wildfire activity has been unprecedented during the past four decades, evidenced by the total area burned in Western forests increasing by 1270% since the 1970s (Abatzoglou and Kolden, 2013; Abatzoglou and Williams, 2016; Westerling, 2016). Because 65% of the West's water supply is sourced from forested lands under elevated fire risk (Brown et al., 2008) and the West's water is almost completely allocated (Hurd and Coonrod, 2012), quantifying the impact of fire on water supplies is becoming increasingly consequential. Projected increases in demand and changes in the magnitude and timing of supply as a result of climate change are expected to lead to regular water shortages by the middle of the century if major adaptations are not implemented (Foti et al., 2012; Blanc et al., 2014; Chavarria and Gutzler, 2018; Brown et al., 2019).

Wildfires can alter watershed hydrology in several ways, with the most significant changes evident in high severity burns (Martin and Moody, 2001). Following combustion of the forest canopy, undergrowth, ground litter, and interception storage diminishes, resulting in elevated throughfall (Veatch et al., 2009; Williams et al., 2019b). Additionally, infiltration is reduced via the development of water-repellent soils (Debano, 2000; Nyman et al., 2010; Moody and Ebel, 2012), soil sealing by ash and fine sediment (Onda et al., 2008; Larsen et al., 2009; Nyman et al., 2014), loss of soil structure (Neary et al., 1999, Moody et al, 2016), and reduction in macropores (Nyman et al., 2014). The removal of mature vegetation also greatly reduces transpiration (Nolan et al., 2014; Poon and Kinoshita, 2018; Blount et al., 2020) but increases

soil evaporation, usually resulting in a net reduction in evapotranspiration (ET) (Paco et al., 2009; Schlesinger and Jasechko, 2014; Mankin and Patel, 2023). However, ET may increase or remain unchanged following fire in areas with high total radiation and/or rapid regrowth of post-fire vegetation (Goeking and Tarboton, 2020). Furthermore, elevated radiative and turbulent energy fluxes typically increase the rate and advance the timing of snowpack ablation (Veatch et al., 2009; Burles and Boon, 2011; Harpold et al., 2014; Giovando and Niemann, 2022).

The changes in watershed hydrology often result in notable differences between pre- and post-fire streamflow behavior (Helvey, 1980; Kinoshita and Hogue, 2015; Bart and Tague, 2017; Moeser and Douglas-Mankin, 2021; Mankin et al., 2022), but the impacts are highly variable. Past studies have demonstrated that a single wildfire can affect the full spectrum of streamflow conditions, ranging from baseflow to flood events. For example, Helvey (1980) demonstrated that post-fire streamflow at all observed frequencies more than doubled in a severely burned forested watershed in central Washington. In contrast, Bart and Hope (2010) found no detectable change in post-fire streamflow using a paired-catchment approach in a central California watershed that was 100% burned (53% moderate to high severity). Additionally, the duration of the wildfire's effect on streamflow is highly variable, ranging from no measurable effect (Bart and Hope, 2010), to less than five years (Hubbert et al., 2012), to more than four decades (Niemeyer, 2020). While there is no clear agreement, the proportion of the watershed burned, burn severity, post-fire precipitation, and vegetative regrowth are believed to be the primary controls on the magnitude of change in post-fire hydrologic responses (Kinoshita and Hogue, 2011; Bart and Tague, 2017; Wagenbrenner et al., 2021). However, the rainfall-streamflow relationship is highly complex and focusing on a single factor may be insufficient to account for changes in streamflow after fire. Bart (2016) concluded that incorporating multiple variables

(e.g., annual streamflow from unburned watersheds, percentage of watershed burned, vegetative recovery, etc.) in a model improved its ability to predict post-fire streamflow compared to using the variables individually.

The effect of wildfire on streamflow has been studied for nearly a century (Hoyt and Troxel, 1934), but only in the last decade have methods been employed to isolate the effect of fire from other factors. Bart (2016) demonstrated that annual streamflow from unburned control watersheds is a highly significant predictor of annual streamflow in burned watersheds, demonstrating that non-fire-related factors and regional weather patterns strongly influence streamflow response after fire. To expound upon this, a number of recent wildfire hydrology studies have introduced a residual term that captures changes in streamflow attributed to disturbance (i.e., wildfire) while accounting for other components that affect streamflow (i.e., climate, etc.) separately (Williams et al., 2022). Hallema et al. (2017) utilized a double-mass analysis and climate elasticity model framework to separate streamflow contributions attributable to fire (residual term) and climate by linearly relating changes in mean annual streamflow to relative changes in mean annual precipitation. In doing so, they estimated that a burned watershed in Arizona experienced a 266% increase in annual yield in the 5 years after fire, where +219% was attributed to fire and the other +47% was attributed to meteorological conditions. Using the same methodology, they estimated that a burned watershed in California experienced a -64% change in annual yield in the 5 years after fire, where +38% was attributed to fire and -102% was attributed to meteorological conditions. Another way to isolate the effect of the fire is to quantify all sources and sinks in the system of interest. Taking this approach, Blount et al. (2020) estimated the residual term on an annual basis by quantifying precipitation, streamflow, ET, and subsurface storage for pre- and post-fire time periods in a burned watershed in Western

Montana. By assuming identical annual climatic conditions during the pre- and post-fire periods, they estimated that the net reduction in ET and increased subsurface storage attributable to the fire resulted in a +140% increase in streamflow during the 11-year post-fire study period.

So far, the studies using the residual approach have utilized monthly or annual streamflow data to evaluate changes due to fire (Mahat et al., 2016; Hallema et al., 2017; Blount et al., 2020; Williams et al., 2022). However, because temporal variations in precipitation play a key role in generating streamflow (Shuai et al., 2022), increasing the temporal resolution could provide a clearer indication of the wildfire effects while also highlighting seasonal or event-based changes in behavior. Furthermore, prior research has estimated the residual term using data analysis methods (Mahat et al., 2016; Hallema et al., 2017; Blount et al., 2020; Williams et al., 2022). Watershed models have the potential to improve upon the past methodology because they are able to account for the numerous, interconnected physical processes that directly influence streamflow (i.e., actual ET, soil processes, interception storage, interflow, etc.).

The primary objective of this study is to isolate and quantify the effect of wildfire on streamflow at a daily resolution over multiple years by combining measured streamflow and simulations from a watershed model. The study considers six watersheds affected by wildfires. For each watershed, a model is used to estimate the streamflow that would have occurred during the post-fire period had the wildfire not happened. Each model is constructed by calibrating to multiple years of measured streamflow in the pre-fire period and then applying the model without changes to the post-fire period. The effect of the wildfire is then estimated as the difference between measured streamflow (burned condition) and simulated streamflow (unburned condition) during the post-fire period. By operating at a daily resolution for multiple years, we identify conditions (e.g., low flow vs. high flow) for which streamflow changed

throughout the recovery of the watershed, which provide insight for post-fire water management strategies.

The outline of this thesis is as follows. Chapter 2 discusses the study watersheds. Chapter 3 highlights modeling methodology. Chapter 4 summarizes the datasets used in this research. Chapter 5 presents the simulated streamflow data for the study watersheds and discusses implications of these results, and Chapter 6 provides the main conclusions of the study.

# 2. STUDY WATERSHEDS

The following criteria were used to select the study watersheds: (1) availability of daily USGS stream gauge data before and after the wildfire of interest, (2) absence of reservoirs or diversion structures upstream of the stream gauge, (3) low fire activity prior to the wildfire of interest, (4) at least 50% of the watershed burned in the wildfire of interest, and (5) the wildfire of interest occurred no earlier than 1985 to allow the use of gridded meteorological data. These five criteria yielded over 40 potential study watersheds. The final selection was made based on the quality of the input data, the severity of the wildfire, and the length of pre- and post-fire records. The six watersheds selected for this study have nearby meteorological stations, wildfires with a high fraction of moderate to high burn severity area, and lengthy pre-fire and post-fire records (Table 1).

## 2.1 North Eagle Creek

North Eagle Creek is an intermittent stream on the eastern slopes of the Sierra Blanca Range in south central New Mexico, U.S. (Figures 1a, 1b). The 13.9 $km^2$ watershed has an average slope of 48%, and elevations from 2,330 to 3,250 m. The wildfire of interest, the June/July 2012 Little Bear Fire, burned 93% of the watershed, with moderate to high severity burns covering 34% of the watershed (MTBS, 2022). Only one other fire (2003 Ski Run Fire; 6.6% of watershed burned) occurred in the watershed between 1950 (when National Interagency Fire Center records begin) and 2021 (Table A.1 provides the fire history for each watershed) (NIFC, 2022). Prior to the Little Bear Fire, vegetation was Douglas fir, ponderosa pine, lodgepole pine, and aspen (USGS, 2022a). The Sierra Blanca soil complex consists of Oligocene-era pyroclastics, lava flows, and intrusions (Kelley et al., 2014). Although an official soil survey is unavailable for the study area, a limited number of soil profiles taken during field

reconnaissance were classified as gravelly clay loams 75 cm in depth. Average annual precipitation (1981 to 2021) is 810 mm, with 60% of this total occurring during the summer monsoon season (June-September) (Daly et al., 2008; PRISM, 2022). Snowpack reaches maximum snow water equivalent (300 mm) in February to March, followed by a rapid ablation period (NRCS, 2022a). The watershed has been considered in previous wildfire/streamflow studies by Moeser and Douglas-Mankin (2021) and Mankin et al. (2022).

### 2.2 Lopez Creek

Lopez Creek is a perennial stream in the Santa Lucia Range in coastal central California, U.S. (Figures 1a, 1c). The 54.0 $km^2$ watershed has an average slope of 52% and elevations range from 180 to 870 m. The wildfire of interest, the July 1985 Las Pilitas Fire, burned 100% of the watershed with 53% experiencing moderate to high severity burns (MTBS, 2022). Only 2.0% of the watershed burned before the Las Pilitas fire and 0.7% burned afterward (Table A.1) (NIFC, 2022). Prior to the Las Pilitas Fire, the watershed consisted primarily of coastal live oak and savanna and chaparral (USGS, 2022a). Watershed geology is dominated by the Miocene-era Monterey Formation, which is a well-bedded mix of shale, siltstone, and mudstone (Nilsen, 1981). Soil surveys classify local soils as clay loams with gravel 40 to 130 cm in depth (NRCS, 2022b). Average annual precipitation (1981 to 2021) is 680 mm, with 70% of this total occurring during winter and early spring (November-March) (PRISM, 2022). Snowfall is exceptionally rare because precipitation rarely falls at temperatures below 0°C (PRISM, 2022). The watershed has been considered in a previous wildfire/streamflow study by Bart and Hope (2010).

### 2.3 San Bernardino Watersheds

Four neighboring watersheds in the San Bernardino Range (Devil Canyon Creek, Plunge Creek, East Twin Creek, and City Creek) in southern California, U.S. were affected by the same

wildfire of interest: the October/November 2003 Old Fire (Figures 1a, 1d). Prior to the Old Fire, vegetation consisted of chaparral, ponderosa pine, lodgepole pine, and oak (USGS, 2022a). Local geology is highly complex with Cretaceous-era granites folded and faulted across a metamorphosed core of Precambrian gneiss (Morton and Miller, 2006). Long-term average annual precipitation (1981 to 2021) is 650 mm, with 80% occurring during winter and early spring (November to March) (PRISM, 2022). Snow regularly falls in the winter above 1000 m in elevation considering that precipitation often falls at temperatures below 0°C (PRISM, 2022).

Devil Canyon Creek

The Devil Canyon Creek watershed has an area of 14.5 $km^2$, with an average slope of 50% and an elevation range from 630 to 1650 m. Prior to the fire, Devil Canyon Creek was perennial during wet years and intermittent during dry and average precipitation years. The Old Fire burned 96% of the watershed, with moderate to high severity burns covering 71% (MTBS, 2022). Two notable wildfires, the 1954 and 1980 Panorama Fires, burned 90% and 27% of the watershed, respectively, before the Old Fire (Table A.1) (NIFC, 2022). Less than 1% of the watershed has burned since the Old Fire (NIFC, 2022). Soil surveys suggest that local soils are primarily gravelly or sandy loams 90 cm in depth (NRCS, 2002b). The watershed has been considered in previous wildfire/streamflow studies, notably by Kinoshita and Hogue (2011), and Kinoshita and Hogue (2015).

City Creek

The City Creek watershed has an area of 51.5 $km^2$, with an average slope of 47% and an elevation range from 440 to 1970 m. Prior to the fire, City Creek was perennial. In 2003, the Old Fire burned 84% of the watershed with moderate to high severity burns covering 58% (MTBS, 2022). Earlier in the same year, 10% of the watershed was burned by the Bridge Fire, with 6% of

the watershed experiencing moderate to high severity burns (MTBS, 2022). Before the Old Fire, East Highland (1956), McKinley (1956), Bear (1970), and Sycamore (1980) Fires, burned 21%, 60%, 28%, and 14% of the watershed, respectively (Table A.1) (NIFC, 2022). Only 5% of the watershed burned after the Old Fire (NIFC, 2022). Soil surveys suggest that local soils are gravelly sandy loams, 40 to 150 cm in depth (NRCS, 2022b). The watershed has been considered in previous wildfire/streamflow studies including Kinoshita and Hogue (2011) and Kinoshita and Hogue (2015).

East Twin Creek

The East Twin Creek watershed has an area of 23.6 $km^2$, with an average slope of 49% and elevation range of 490 to 1870 m. Prior to the fire, East Twin Creek was perennial. The 2003 Old Fire burned 94% of the watershed with moderate to high severity burns covering 43% (MTBS, 2022). Moreover, 43% of the watershed burned in the 2002 Arrowhead Fire, with 11% of the watershed experiencing moderate to high severity burns (MTBS, 2022). Before the Old Fire, Arrowhead Springs (1953) and Panorama (1980) Fires burned 55% and 83% of the watershed, respectively (NIFC, 2022) (Table A.1). Less than 1% of the watershed has burned since the Old Fire (NIFC, 2022). Soil surveys suggest that local soils are composed of gravelly sandy loams 40 to 150 cm in depth (NRCS, 2022b).

Plunge Creek

The Plunge Creek watershed has an area of 43.4 $km^2$, with an average slope of 44% and an elevation range of 520 m to 2000 m. Prior to the fire, East Twin Creek was perennial during wet years and intermittent during dry and average precipitation years. The Old Fire burned 49% of the watershed, with moderate to high severity burns covering 21% (MTBS, 2022). Before the Old Fire, Smiley (1955), East Highland (1956), Bear (1970), and Mill (1997) Fires, burned 10%,

44%, 82%, and 12% of the watershed, respectively (Table A.1) (NIFC, 2022). After the Old Fire, 24% of the watershed burned again in the 2007 Slide Fire (NIFC, 2022). Soil surveys suggest that local soils are gravelly sandy loams 40 to 150 cm in depth (NRCS, 2022b).

# 3. MODELING METHODOLOGY

We calibrated a model for each watershed for pre-fire conditions and then used the model to simulate the daily post-fire streamflow that would have occurred without wildfire. A residual term, the difference between the measured streamflow (burned condition) and the simulated streamflow (unburned condition), was used to isolate the effect of wildfire on streamflow during the post-fire period.

## 3.1 Model Description

Modeling was performed using the Ages model (version 1.0). Ages is a watershed model that implements hydrologic and ecological components into one framework (Ascough et al., 2012; Green et al., 2015). Its components were adapted from the J2000 and J2000-SN (Krause, 2002; Nepal et al., 2014), SWAT (Arnold et al., 2012), WEPS (Wagner, 2013), and RZWQM (Ma et al., 2012) models. Ages has shown promise relative to other watershed models (i.e., PRMS and SWAT) in mountainous environments, potentially due to representation of ET losses, soil-water distribution, and surface and subsurface hydrologic response unit (HRU) connectivity that mirrors the complex hydrologic processes and interconnections in mountain forest environments (Mankin et al., 2022). The model was used with a daily time step. Spatial variability was considered by dividing each study basin into HRUs that were delineated based upon stream network patterns. The minimum size of each HRU was held at 100 ha; smaller areas were merged until the size exceeded 100 hectares.

Daily meteorological inputs included precipitation, air temperature, relative humidity, wind velocity, and shortwave solar radiation. These variables were interpolated to the centroid of each HRU via an inverse distance weighting method before use on the model. Ages partitions precipitation between rain, snow, or a mix, depending upon air temperature. Actual (simulated)

ET is determined from simulated soil moisture and Penman-Monteith potential ET, where longwave radiation is calculated from the air temperature, actual vapor pressure, shortwave solar radiation, and the clear sky solar radiation (Ascough et al., 2012). Albedo and crop coefficient values are based upon the default Ages values for the land classification of each respective HRU (Neitsch et al., 2011).

Precipitation is first intercepted by the canopy and is assumed to exit the system at the potential ET rate. Canopy interception storage ($s_{\text{canopy}}$, mm) uses the simple storage approach described in Dickinson (1984), which is a function of the leaf area index (LAI) ($A$, $m^2/m^2$) and the storage capacity of the leaf area ($\alpha_{rain,snow}$, mm):

$$s_{canopy} = A\alpha_{rain,snow} \quad (1).$$

where α has separate values for snow and rain. If $s_{canopy}$ is exceeded, surplus precipitation is treated as throughfall and passed to other modules (i.e., soil water and/or snow).

The snow module is adapted from the model described in Knauf (1980), which simulates the different phases of accumulation, metamorphosis, and melt. The snow module has an emphasis on changes in snow density due to melting and subsidence, which allows it to store free water until a certain threshold density is reached. During the lifetime of the snowpack, the model switches between the accumulation and compaction/melt phases, depending upon air temperature. Two temperature thresholds are established. If the air temperature is below the accumulation threshold and precipitation only falls as snow, only the accumulation phase is active. If the air temperature is above the melt threshold and precipitation only falls as rain, only the compaction/melt phase is active. Between the two temperatures, or if precipitation falls as a mix of rain and snow, both phases are active. Stored energy in the snowpack is considered with

cold content, which prevents snowmelt from occurring until cold content exceeds a value of zero. The amount of potential snowmelt ($m$, mm) which occurs is given by:

$$m = T_{air} p_{tfactor} + T_{air} p_{rfactor} r + p_{gfactor} \quad (2)$$

where $T_{air}$ is air temperature (ºC), $p_{tfactor}$ is a calibrated parameter describing energy input from air temperature (mm/°C), $p_{rfactor}$ is a calibrated energy input parameter from rain (mm/°C), $p_{gfactor}$ is a calibrated energy input parameter from soil heat flow (mm), and $r$ is the depth of rain (mm). The snowpack is able to store liquid water up to a certain critical density ($\rho_{crit}$, $\mathrm{g/cm^3}$), beyond which water is released from the snowpack. The maximum SWE the snowpack can store ($W_{max}$, mm) is calculated by:

$$W_{max} = \frac{\rho_{crit}}{\rho_{water}} d \quad (3)$$

where $\rho_{water}$ is the density of water ($\mathrm{g/cm^3}$) and $d$ is the depth of the snowpack (mm). Water stored in the snowpack which exceeds $W_{max}$ is converted to runoff ($Q_{snow}$, mm) by:

$$Q_{snow} = W_{tot} - W_{max} \quad (4)$$

where $W_{tot}$ is total SWE (mm). The density of the snowpack is then held at the critical density until it either completely melts or accumulation occurs from new snowfall.

Soil water is the most complex module in Ages and interacts with nearly all other modules. Actual infiltration ($i_{\mathrm{act}}$, mm/d) of rainfall, ponded surface water, or snowmelt is computed by:

$$i_{\mathrm{act}} = i_{\mathrm{max}}(1 - \theta_{\mathrm{soil}}) + k_{\mathrm{f}} \quad (5)$$

where $i_{\mathrm{max}}$ is a maximum possible infiltration rate (mm/d), $\theta_{\mathrm{soil}}$ is the degree of soil water saturation in the respective layer ($\mathrm{m^3/m^3}$), and $k_{\mathrm{f}}$ is the field saturated hydraulic conductivity of

the uppermost soil layer (mm/d) (Green et al., 2015). Any water exceeding $i_{\mathrm{act}}$ is passed to soil depression storage, which may either infiltrate or evaporate. If soil depression storage capacity is exceeded, surplus water is routed to the nearest channel or HRU. Once water enters the soil profile, it is partitioned between two compartments, middle pore storage (MPS) and large pore storage (LPS), in the unsaturated zone. MPS represents the water stored in medium-sized pores (diameter = 0.2 to 50 μm), which can be held against gravity (i.e., field capacity). LPS represents the water held in large pores and macropores (diameter > 50 μm), which cannot be held against gravity (i.e., air capacity). MPS can only be removed via suction (i.e., transpiration), while LPS can be removed by transpiration, interflow, and percolation. The distribution of infiltrated water between the MPS ($M_{\mathrm{in}}, \mathrm{mm/d}$) and LPS ($L_{\mathrm{in}}, \mathrm{mm/d}$) is calculated using the degree of soil water saturation of the MPS ($\theta_{\mathrm{MPS}}$, $\mathrm{m^3/m^3}$) as an indicator:

$$M_{\mathrm{in}} = i_{\mathrm{act}}\left(1 - \mathrm{e}^{-p_{distMPSLPS}/\theta_{\mathrm{MPS}}}\right) \quad (6)$$

$$L_{\mathrm{in}} = i_{\mathrm{act}} - M_{\mathrm{in}} \quad (7)$$

where $p_{distMPSLPS}$ is a calibrated parameter that controls the distribution of infiltration to MPS and LPS. The total outflow rate from the LPS ($L_{\mathrm{out}}, \mathrm{mm/d}$) is given by:

$$L_{\mathrm{out}} = L_{\mathrm{act}}\theta_{\mathrm{soil}}^{p_{LPSout}} \quad (8)$$

where $L_{\mathrm{act}}$ is the maximum available outflow in LPS (mm/d) and $p_{LPSout}$ is a calibrated parameter for LPS outflow.

Interflow ($I$, mm/d) and percolation ($P$, mm/d) are calculated using the HRU slope ($S$) and pedological parameters (e.g., thickness of soil layers and hydraulic conductivity):

$$I = L_{\mathrm{out}} p_{latVertDist} \tan S \quad (9)$$

$$P = L_{\text{out}} p_{latVertDist} \tan(1 - \tan S) \tag{10}$$

where $p_{latVertDist}$ is a calibrated parameter that controls the distribution between interflow and percolation. Actual ET ($E_{\text{act}}, \text{mm/d}$) is calculated based on potential ET ($E_{\text{pot}}, \text{mm/d}$) and degree of saturation of the MPS ($\theta_{\text{MPS}}$) via a polynomial reduction function:

$$E_{\text{act}} = E_{\text{pot}}\, 10^{-\frac{10(1-\theta_{\text{MPS}})}{p_{SoilPolRed}}} \tag{11}$$

where $p_{SoilPolRed}$ is a calibrated ET reduction factor.

Groundwater is divided into two storages: fast-moving shallow groundwater and slow-moving deeper groundwater:

$$G_{1\text{in}} = p_{\text{distMPSLPS}} P \tan S \tag{12}$$

$$G_{2\text{in}} = p_{\text{distMPSLPS}} P (1 - \tan S) \tag{13}$$

where $G_{1\text{in}}$ is shallow aquifer recharge (mm/d) and $G_{2\text{in}}$ is deep aquifer recharge (mm/d). Groundwater outflow (i.e., baseflow) is a function of storage content and a recession constant:

$$G_{1\text{out}} = \frac{G_{1\text{act}}}{k_{\text{G1}}} \tag{14}$$

$$G_{2\text{out}} = \frac{G_{2\text{act}}}{k_{\text{G2}}} \tag{15}$$

where $G_{1\text{out}}$ is shallow aquifer outflow (mm/d), $G_{2\text{out}}$ is deep aquifer outflow (mm/d), $G_{1\text{act}}$ is shallow aquifer storage content ($\text{m}^3/\text{m}^3$), $G_{2\text{act}}$ are deep aquifer storage content ($\text{m}^3/\text{m}^3$), and $k_{\text{G1}}$ and $k_{\text{G2}}$ are calibrated recession coefficients.

Following the calculation of surface streamflow, interflow, and baseflow, combined water fluxes are computed based on topological interconnections. Topological routing files for Ages are generated by the Cadel (Catchment areas delineation) tool (Kipka et al., 2019).

Streamflow paths and HRUs are generated from digital elevation model (DEM) raster data at user-specified resolutions. Land cover and soils can vary from one HRU to the next. For this research, the National Land Cover Database (NLCD) pre-fire land cover and Web Soil Survey soil type that covered the highest percentage of the respective HRU area were assigned to each HRU. The topology routing scheme allows for multiple streamflow-path directions as well as interactions between neighboring HRUs. Water can flow (1) on the surface as runoff on the surface following topography, (2) laterally as interflow between soil horizons, (3) vertically from the vadose zone to the water table, (4) laterally as groundwater between HRUs, and (5) as discharge into or out of stream channels. Channel routing is performed by applying the kinematic wave approach and streamflow is then iteratively calculated via the Manning-Strickler equation. Finally, stream reach outflow, $Q_{\text{out}}$ ($\text{m}^3/\text{s}$), is calculated from streamflow velocity, $v$ (m/s), streamflow in the stream reach, $q_{\text{act}}$ ($\text{m}^3/\text{s}$), and a unitless flood routing coefficient, $r_{\text{k}}$:

$$r_{\text{k}} = \frac{3600 v t_a}{l} \tag{16}$$

$$Q_{\text{out}} = q_{\text{act}} \cdot \text{e}^{\left(-\frac{1}{r_{\text{k}}}\right)} \tag{17}$$

where $t_a$ is a calibrated routing coefficient and $l$ (m) is the streamflow length of the respective stream reach.

### 3.2 Model Calibration and Evaluation

The model for each of the six watersheds was simulated for a warmup period prior to the calibration period. This was done to limit the effect of unknown initial values for MPS, LPS, groundwater storage, etc. The warmup period for all watersheds except Lopez Creek was two years in duration. The warmup period for Lopez Creek was shorter than the others (1 month) due to the limited availability of earlier meteorological input data.

Calibration was performed using LUCA (Let us calibrate) (Hay and Umemoto, 2006), a shuffled complex evolution calibration tool, by comparing simulated daily streamflow with measured daily streamflow. LUCA operates within a specified range of plausible parameter values. Weights were assigned to different objective functions, which included Nash-Sutcliffe efficiency (NSE), NSE calculated on the log of streamflow (NSE-Log), and Kling-Gupta efficiency (KGE). Because NSE has been shown to emphasize high flows (Clark et al., 2021) and NSE-Log cannot be calculated when observed flows are zero, observed flows of zero were replaced by a value of 0.1 L/s. This substitution allowed NSE-Log to be calculated at all times and thus ensured that the calibrated model considers the full record of observed streamflow. Ages relies heavily on the calibration process, as nearly every parameter of significance was calibrated. A total of 52 parameters were calibrated, and the final values for each watershed are given in Table B.1 and B.2. An example of the calibration scheme is provided in Appendix C.

Before performing the final calibration for each basin, a split sample procedure was used to evaluate the model's reliability for estimating streamflow for unobserved periods. For each watershed, the pre-fire streamflow was divided approximately evenly between preliminary calibration (Split 1) and evaluation (Split 2) datasets. While wet and dry periods were included in each dataset to the extent possible, Split 1 was still much wetter than Split 2 for every watershed. The final pre-fire calibration periods for each watershed used both Split 1 and 2. The final calibration period varied according to data availability: North Eagle Creek (4.7 years), Lopez Creek (4.4 years), Devil Canyon Creek (9.1 years), City Creek (8.9 years), East Twin Creek (7.7 years), and Plunge Creek (9.1 years). Calibration periods for City Creek and East Twin Creek were less than Devil Canyon Creek and Plunge Creek due to the potentially non-negligible effects of the 2003 Bridge and 2002 Arrowhead fires.

# 4. DATASETS

## Meteorological Data

While weather stations were present within a few kilometers of the study basins, gridded surface meteorology datasets were chosen to capture orographic variability within the mountainous watersheds. Three gridded datasets were utilized in this research because no single source included all the required climate variables. Average daily incident shortwave radiation was obtained from Daymet (version 4 R1) (Thornton et al., 2021). Average daily wind speed was obtained from GridMET (Abatzoglou, 2013). Daily minimum and maximum temperatures, average relative humidity, and precipitation were obtained from PRISM (PRISM, 2022). All meteorological datasets have 4 km grid cells. Both Daymet and GridMET define a day as "midnight to midnight local standard time" (Thornton et al., 2021; Abatzoglou, 2013), which is consistent with the model's daily time step. However, PRISM defines a day as "the 24 hours ending at 12:00 Greenwich Mean Time" (PRISM, 2022). Because the study watersheds are in the Mountain and Pacific time zones, unaltered PRISM data include only 4 or 5 hours of data from the day of interest. Therefore, PRISM data were shifted one day earlier (e.g., data listed by PRISM as May 26 were recategorized as May 25) to improve their overlap with the other datasets.

## Soil Data

Soil data were obtained from the Natural Resources Conservation Service's Web Soil Survey (NRCS, 2022b). Ages allows for soil units to vary between HRUs. If an HRU had more than one soil unit within its boundaries, the soil unit with the largest coverage in the HRU was assigned as the sole unit. The range of values used by the LUCA calibration process for layer

thickness, porosity, field capacity, wilting point, and infiltration capacity were constrained based upon values presented by the Web Soil Survey.

Land Cover Data

National Land Cover Database (NLCD) data were obtained for 2001, 2003, 2006, 2008, 2011, 2013, 2016, and 2019 to track vegetative recovery following the fires (USGS, 2022a). Land cover used in the model for North Eagle Creek and the San Bernardino watersheds were based on the most recent NLCD dataset before the fire (i.e., 2011 and 2001, respectively). Because NLCD products were unavailable prior to 2001, the land cover for the Lopez Creek model was based upon the 2019 NLCD dataset (based on the assumption that the vegetation 35 years after the fire would be similar to pre-fire conditions). Land cover data for the post-fire analysis for Lopez Creek were obtained from LCMAP from 1985 to 2010 (USGS, 2022b).

Leaf Area Index

LAI data were obtained from data collected by the NASA Moderate Resolution Imaging Spectroradiometer (MODIS) satellite. LAI is calculated using algorithms that consider spectral reflectances, land cover type, and information on biomes and soil patterns (Myneni et al., 2002). Data from September were used because September has been found to approximately represent average annual LAI values in evergreen forests, grasslands, and shrublands (Ukasha et al., 2022). LAI data throughout the month of September were obtained each year from 2002 to 2021 for each watershed.

Fire Data

Historic fire perimeters were collected from the National Interagency Fire Center and are available from 1950 to 2022 (NIFC, 2022). Burn severity data were obtained from Monitoring

Trends in Burn Severity (MTBS) (MTBS, 2022). While burn severity data from Burned Area Emergency Response (BAER) were considered for use in this study, BAER does not date back to the 1985 Las Pilitas Fire. Thus, MTBS data were used for all watersheds for consistency. MTBS burn severity data are created by first calculating a Normalized Burn Ratio (NBR) from near-infrared and shortwave infrared spectral ranges. Then, the difference between pre-fire and post-fire NBR images is classified into burn severity classes (Eidenshink et al., 2007). For these reasons, MTBS emphasizers the burn severity of vegetation and does not provide detail on burn severity of soil layers.

Streamflow Data

USGS streamflow data were obtained for each study basin from the first day of record through December 31, 2021 (USGS, 2022c). The time series of daily streamflow for North Eagle Creek was constructed via subtraction of the South Eagle Creek near Alto, NM (USGS 08387575) stream gauge from the Eagle Creek below South Fork near Alto, NM (USGS 08387600) stream gauge. The two stream gauges are located just upstream and downstream of the confluence of the North and South Forks and within 100 m of one another. The other stream gauges used in this study directly measure the streamflow at the study basin outlets. They include Lopez Creek near Arroyo Grande, CA (USGS 11141280), Devil Canyon Creek near San Bernardino, CA (USGS 11063680), East Twin Creek near Arrowhead Springs, CA (USGS 11058500), City Creek near Highland, CA (USGS 11055800), and Plunge Creek near East Highlands, CA (USGS 11055500).

# 5. RESULTS AND DISCUSSION

Calibration performance statistics are summarized in Table 2. Performance statistics were generally better during the wetter calibration (Split 1) periods than the drier evaluation (Split 2) periods. The difference may suggest that Ages performs better during wet conditions than dry conditions, but it also may suggest that Ages is prone to overfitting due to its large number of calibrated parameters. Even with the drop in performance for the evaluation periods, the split sample analysis suggests that the model can produce useful predictions for unobserved periods (upper part of Table 2). The final calibration models (lower part of Table 2) also accurately reproduced daily streamflow for the pre-fire periods. All models had final calibration NSE values of 0.85 or greater and bias values 4.0% or less, indicative of very good model performance (Harmel at al., 2018) except Lopez Creek, which had NSE = 0.65, indicating satisfactory to good performance. All models except the two intermittent San Bernardino watersheds, Devil Canyon Creek and Plunge Creek, had final calibration NSE-Log values of 0.5 or greater, indicating satisfactory performance under lower-flow conditions.

## 5.1 North Eagle Creek

Annual average precipitation was nearly identical between the pre-fire (721 mm/yr) and post-fire (731 mm/yr) periods. Prior to the June/July 2012 Little Bear Fire, North Eagle Creek was an ephemeral/intermittent system (Figure 2a). In general, streamflow only occurred during summer monsoon and early spring snowmelt periods. For the remainder of the year, streamflow generally dropped below the detectable limit of the stream gauge. Zero-flow conditions were recorded for 62% of the 4.7-yr pre-fire period. Flow conditions varied considerably from year to year. Both 2008 and 2010 were active monsoon seasons, resulting in extended periods of continuous streamflow, including an historically large rainfall event in July 2008. The period

between 2011 and 2012 was very dry, with only 5 days of recorded streamflow in the final 471 days before the fire. Snowmelt-driven streamflow usually occurred for about a month at intermediate streamflow rates (i.e., <10 L/s). The only exception to this was in 2010, which saw about four months of higher streamflow (i.e., >10 L/s) driven by snowmelt.

For the pre-fire period, the model usually accurately reproduced periods of zero flow and high flows but was less accurate for non-zero streamflow events below 20 L/s (Figures 2a, 3a), typically simulating zero flow within that range. Flow duration curves (FDCs) of measured and simulated streamflow during the pre-fire period confirmed accurate simulation of high flows but underestimation of low flows for the pre-fire period (Figure 3a). Note that the curves do not reach 100% exceedance probability (EP) due to the occurrence of zero-flow conditions. The difference between the two curves confirms that the model accurately reproduced high flows while underestimating low flows for the pre-fire period.

Measured streamflow patterns visibly shifted between the pre-fire (Figure 2a) and post-fire periods (Figure 2b). Mean streamflow and 30-day maximum streamflow were 150% and 78% higher, respectively, for the post-fire period. The 30-day minimum streamflow increased from 0 to 0.4 L/s. Non-zero flow was recorded 57% more frequently in the post-fire period.

The post-fire period (PFP) (9.4 years) was subdivided into three successive periods based upon differences between measured (burned condition) and simulated (unburned condition) streamflow: PFP-1 (2.0 years), PFP-2 (1.9 years), and PFP-3 (5.5 years) (Table 1). During PFP-1, measured (burned) streamflow remained ephemeral and was slightly elevated relative to simulated (unburned) streamflow (Figure 2b). FDCs indicate that the magnitude of all non-zero flows increased due to fire (Figure 3b); however, it is probable that the simulations underestimated the low flows for all post-fire periods similar to the pre-fire simulations (Figures

3a, 3b). Therefore, it is likely that flows between 0% and 10% EP experienced an increase due to the fire.

North Eagle Creek became a perennial stream throughout PFP-2 while the simulated (unburned) streamflow remained ephemeral (Figure 2b), even with an increase in precipitation of 66% relative to PFP-1. Non-zero streamflow was measured on 98% of days compared to 50% for simulated conditions. Measured streamflow increased relative to simulated (unburned) condition at all EPs (Figure 3c). Specifically, low (>20% to 100% EP), intermediate (>5% to 20% EP), and high (0% to 5% EP) streamflow and annual yield increased by 28,000%, 1,500%, 160%, and 420%, respectively.

Measured (burned) streamflow in PFP-3 remained elevated relative to simulated (unburned) conditions but became intermittent (Figure 2b). Non-zero streamflow was measured on 62% of days compared to 27% for simulated conditions. Measured streamflow increased relative to simulated streamflow at all EPs with non-zero flow (Figure 3d). Low, intermediate, and high streamflow and annual yield increased by 44,000%, 28,000%, 1,600%, and 3,000%, respectively.

North Eagle Creek Discussion

Vegetation was greatly altered by fire, evidenced by average LAI across the watershed decreasing from 2.0 in the pre-fire period to 1.2 in the post-fire period (Figure 4). This reduction in LAI is supported by NLCD data, which showed a watershed-wide shift from 93% evergreen forest in 2011 (1 year before the fire) to 58% evergreen forest, 6% shrub/scrub, and 34% herbaceous in 2013 (1 year after the fire, in PFP-1). More recently, in 2019 (PFP-3), the watershed was 52% evergreen forest, 45% shrub/scrub, and 1% herbaceous.

While streamflow varied substantially between the pre-fire period and all post-fire periods, the most noticeable changes occurred in PFP-2 and PFP-3. In PFP-1, substantial reductions in basin-wide transpiration rates likely occurred due to the drop in LAI. Water that would have been transpired was instead progressively added to subsurface storage throughout PFP-1. The elevated subsurface water content at the beginning of PFP-2 then resulted in elevated baseflow and interflow in PFP-2 and PFP-3. Storm runoff also increased in PFP-2 and PFP-3 due to the inverse relationship between subsurface water content and infiltration capacity. LAI steadily increased throughout PFP-1 (0.9 to 1.2) and PFP-2 (1.2 to 1.4) and then plateaued during PFP-3 (1.4) (Figure 4). This behavior indicates that LAI (and transpiration) may have recovered/increased enough by the beginning of PFP-3 to allow North Eagle Creek to transition back to intermittent, albeit elevated, streamflow.

Mankin et al. (2022) compared calibrated pre- and post-fire model parameters to provide insights into changes in hydrologic processes that may explain changes in rainfall-runoff response. Relative to the pre-fire period, Ages post-fire calibrated parameters required substantial changes to represent interception storage, ET, and soil water processes. Leaf interception storage for rain and snow events decreased by 100% and 26%, respectively, in the post-fire period. This change was confirmed during field reconnaissance in April 2021 during which we found that the vast majority of trees were killed during the Little Bear Fire and remained devoid of leaves or needles that could intercept precipitation. Furthermore, the two Ages parameters that control the magnitude of transpiration were greatly reduced (82% and 97%). Fire also affected several soil water parameters. Soil depression storage and surface soil field capacity were reduced by 97% and 50%, respectively. The reduction in soil depression

storage may reflect the combustion of leaf litter during the fire, while the reduction in field capacity may reflect a loss in soil structure.

### 5.2 Lopez Creek

Annual precipitation for the pre-fire period averaged 922 mm/yr, compared to 720 mm/yr for the post-fire period average. Lopez Creek was a perennial system throughout the pre-fire and post-fire periods (Figures 5a-5c). Large streamflow events, ranging from 1,500 to 15,000 L/s, occurred about 5 to 10 times each year but only in winter and spring (mainly December to March). Due to limited precipitation, only baseflow occurred from spring through fall (April-October), but it rarely dropped below 50 L/s. Nearly all streamflow conditions were adequately modeled. Additionally, nearly every streamflow event was simulated without generating any false events. FDCs confirm that the model accurately reproduced the full range of measured streamflow during the pre-fire period (Figure 6a).

Measured streamflow decreased significantly after fire (Figure 5a vs. Figures 5b and 5c). Mean daily, 30-day maximum, and 30-day minimum streamflows were 42%, 31%, and 36% lower in the post-fire period (1985 to 2010) than during the pre-fire period. However, much of this decrease in streamflow during PFP-1 was attributable to lower levels of precipitation during the post-fire period.

The post-fire period (25.5 years) was subdivided into three successive time periods based upon differences between measured (burned condition) and simulated (unburned condition) streamflow: PFP-1 (5.6 years), PFP-2 (5.8 years), and PFP-3 (14.0 years) (Table 1). During PFP-1, measured streamflow often slowly increased from September through December while simulated streamflow exhibited slow declines (Figure 5b). FDCs confirm that the largest differences between the burned and unburned conditions occurred at low streamflow (Figure 6b).

All streamflow between 15% and 100% EP increased in magnitude. Measured low streamflow (>20% to 100% EP) and annual yield increased by 65% and 6%, while intermediate (>5% to 20% EP) and high streamflow (0 to 5% EP) decreased by 5% and 18%, respectively, compared to simulated streamflow. Considering how closely simulated and measured streamflow align in Figure 6b, we believe that these slight decreases represent model error. Assuming low streamflow increased by 65% and intermediate and high streamflow remained unchanged in PFP-1, annual yield would have increased by 19% instead of by 6%.

PFP-2 had lower measured streamflow (burned condition) compared to simulated streamflow (unburned condition) (Figure 5b). The reduction occurred across the full range of measured streamflow (Figure 6c). Low streamflow, intermediate streamflow, high streamflow, and annual yield decreased by 41%, 38%, 48%, and 44%, respectively, compared to simulated streamflow.

During PFP-3, measured and simulated streamflow appear similar in Figure 5c. The two FDCs also look quite similar (Figure 6d). Low, intermediate, and high streamflow and annual yield decreased by only 6%, 12%, 20%, and 15%, respectively, compared to simulated streamflow. While it is unlikely that Lopez Creek would return to identical pre-fire streamflow conditions in PFP-3, some of the differences between measured and simulated data likely represent minor model errors.

Lopez Creek Discussion

The relationship between measured and simulated streamflow at Lopez Creek following the Las Pilitas Fire is quite different in each of the three post-fire periods. Compared to the unburned condition, annual yield increased during PFP-1 (5.6 years), decreased during PFP-2 (5.8 years), and then returned to the pre-fire average during PFP-3 (14.0 years). The increase in

flow during the PFP-1 may be explained by decreases in transpiration, which partitioned additional water into streamflow. The switch from increased to decreased streamflow 6 years after the fire is hypothesized to be weather driven. About 500 mm of rain (67% of annual precipitation) fell in a 30-day period at the beginning of PFP-2 (February and March 1991), which was then followed by 8 years of average to above-average precipitation. The relatively wet conditions may have led to rapid growth in herbaceous and shrub/scrub biomass, resulting in elevated transpiration rates (Goeking and Tarboton, 2020). As precipitation returned to average levels in the PFP-3, biomass and transpiration rates likely returned approximately to pre-fire values, which allowed Lopez Creek streamflow to return approximately to the pre-fire condition about 11 years after the Las Pilitas Fire. While LAI data do not exist to support this hypothesis, LCMAP data indicates that forest coverage steadily increased during PFP-1 (42% to 50% from 1986 to 1990), increased more rapidly during the PFP-2 (50% to 68% from 1990 to 1996), and then began stabilizing during PFP-3 (68% to 74% from 1996 to 2000 and 74% to 75% from 2000 to 2010) (USGS, 2022b). This rapid increase in forest coverage during the wetter PFP-2 supports the hypothesis that weather-driven biomass and transpiration changes may be responsible for the post-fire streamflow patterns at Lopez Creek.

The slight increase in annual yield during PFP-1 aligns with the findings of Bart and Hope (2010). They found no detectable increase in winter (December to February), spring (March to May), or annual yield at Lopez Creek using a paired catchment analysis of monthly and annual data. In general, our results demonstrate that streamflow during PFP-1 increased the most during low streamflow periods during the dry season (i.e., June through November) while often remaining similar to the pre-fire condition during periods of higher streamflow (i.e., December through May). Considering that Bart and Hope (2010) did not closely examine periods

of low streamflow and that annual yield did not change considerably, it is not surprising that they did not detect a change in streamflow. This highlights the benefit of analyzing the full spectrum of flow frequencies; while yield from certain periods may remain practically unchanged following fire, other periods may exhibit noticeable differences.

### 5.3 San Bernardino Watersheds

Devil Canyon Creek

Annual precipitation across the San Bernardino watersheds for the pre-fire period averaged 664 mm/yr, compared to 577 mm/yr for the post-fire period. Prior to the fire, Devil Canyon Creek was perennial during wet years and intermittent during dry and average precipitation years (Figure 7a). Periods of zero flow often occurred from August through October. Measured streamflow clearly differed between the pre-fire and post-fire periods (Figure 7a vs. Figure 7b). The most obvious change was the shift from intermittent to perennial streamflow for the entirety of the post-fire period. On average, 47 days of zero flow were recorded each year during the pre-fire period, while streamflow was recorded every day during the post-fire period. Mean and 30-day maximum streamflow were 5.2% and 21% lower in the post-fire period, respectively, while 30-day minimum streamflow was 140% higher in the post-fire period.

Overall, the model adequately reproduced much of the streamflow record during the pre-fire period. Intermediate and high streamflow was simulated accurately without generating any false peaks (Figure 7a and 8a). Early periods of the baseflow recession limbs were also simulated accurately, but periods of very low flow and/or zero-flow conditions were consistently overestimated (Figure 7a and 8a). However, measuring very low or zero-flow conditions is difficult; it is possible that some of the rapid drops to zero measured streamflow may be due to

hyporheic flow bypassing the stream gauge (Zimmer et al., 2020), which would result in a closer agreement between measured and simulated streamflow during these conditions. Because the model likely still underestimated low streamflow for the pre-fire period, it is likely that low streamflow and annual yield during the post-fire period increased by more than reported in the following results. Similar behavior occurs for the other San Bernardino watersheds.

The post-fire period (18.2 years) was subdivided into two time periods based upon differences between measured (burned condition) and simulated (unburned conditions) streamflow: PFP-1 (13.1 years) and PFP-2 (5.0 years) for all San Bernardino watersheds (Table 1). During PFP-1, measured baseflow often receded slower than simulated streamflow (Figure 7b), particularly in dry years (e.g., 2007 and 2012 to 2015). FDCs (Figure 8b) indicate that measured streamflow was larger than simulated streamflow in all but the lowest 0.1% EP and most notably between 20% and 100% EP. Low (>20% to 100% EP), intermediate (>5% to 20% EP), and high (0% to 5% EP) streamflow and annual yield increased by 160%, 37%, 10%, and 50%, respectively, compared to simulated streamflow.

PFP-2 experienced an increase in all measured streamflow except the highest flows (Figures 7b, 8c). Although measured low streamflow and intermediate streamflow were greater than simulated flows during this period, the changes were less pronounced than during PFP-1. Low streamflow, intermediate streamflow, high streamflow, and annual yield changed by 68%, 16%, -24%, and 14%, respectively.

City Creek

City Creek was perennial for the entire study period, aside from a 2-month period of zero flow in the summer 2018 (Figure 9b). Measured streamflow patterns are not visibly different between the pre-fire and post-fire periods (Figure 9a vs. Figure 9b). Mean and 30-day maximum

streamflow were 3.4% and 1.1% lower in the post-fire period, respectively, but 30-day minimum streamflow was 56% higher in the post-fire period.

During PFP-1, measured streamflow was higher than simulated streamflow (Figure 9b). FDCs (Figure 10b) also indicate that measured streamflow was consistently larger than simulated streamflow (aside from upper and lower 0.1% EP), most notably between 25% and 95% EP. Measured low, intermediate, and high streamflow and annual yield increased by 240%, 85%, 23%, and 59%, respectively.

During PFP-2, streamflow remained elevated from 0 to 75% EP, but the changes were attenuated with respect to PFP-1 (Figure 9b and Figure 10c). Figure 10c suggests that streamflow decreased from 75% to 100% EP; however, we believe that this decrease is an artifact of modeling inaccuracies, evidenced by the same behavior in the pre-fire period (Figure 10a). The same applies to post-fire results at East Twin Creek and Plunge Creek. Measured low, intermediate, and high streamflow and annual yield increased by 79%, 32%, 30%, and 38%, respectively.

East Twin Creek

East Twin Creek was perennial throughout the entire study period (Figure 11a). Measured streamflow patterns are not visibly different between the pre-fire and post-fire periods (Figure 11a vs Figure 11b). However, measured mean, 30-day maximum, and 30-day minimum streamflows were 29%, 27%, and 41% lower in the post-fire period than during the pre-fire period.

For PFP-1, the differences between the measured and simulated hydrographs were similar to the pre-fire period (Figures 11a, 11b). However, PFP-1 experienced a small increase in all measured streamflow above 1% EP (Figure 12b). Measured low streamflow, intermediate

streamflow, high streamflow, and annual yield increased by 24%, 58%, 13%, and 24%, respectively.

During PFP-2, measured streamflow was larger than simulated streamflow between 1% and 60% EP (Figure 12c). Measured low, intermediate, and high streamflow and annual yield increased by 30%, 47%, 10%, and 24%, respectively.

Plunge Creek

Prior to the fire, Plunge Creek was perennial during wet years and intermittent during dry and average precipitation years (Figure 13a). Periods of zero streamflow often occurred throughout August through October. Measured streamflow patterns are visibly different between the pre- and post-fire periods (Figure 13a vs Figure 13b). In particular, the previously intermittent stream remained perennial for the first 13 years of the post-fire period. On average, 43 days of zero flow per year were recorded during the pre-fire period. Mean and 30-day maximum streamflow were 7.3% and 13% lower in the post-fire period, respectively, while 30-day minimum streamflow was 370% higher.

For PFP-1, measured streamflow almost always exceeded simulated streamflow (Figure 13b). FDCs indicate that measured streamflow exceeded simulated streamflow between 1% and 95% EP (Figure 14b). Measured low, intermediate, and high streamflow and annual yield increased by 170%, 50%, 1%, and 30%, respectively.

For PFP-2, measured streamflow was larger than simulated streamflow between 0% and 80% EP (Figures 13b, 14c). Measured low, intermediate, and high streamflow and annual yield increased by 58%, 41%, 34%, and 39%, respectively.

San Bernardino Discussion

The effects of the 2003 Old Fire varied among watersheds. During PFP-1, on an annual basis, Devil Canyon Creek, City Creek, and Plunge Creek all experienced consistently elevated streamflow, whereas increases in streamflow at East Twin Creek were smaller and inconsistent (Figure 15). Throughout PFP-1, measured (burned) low streamflow increased by 160%, 240%, 24%, and 170% and annual streamflow increased by 50%, 59%, 24%, and 30% at Devil Canyon Creek, City Creek, East Twin Creek, and Plunge Creek, respectively, compared to simulated (unburned) conditions. During PFP-2, streamflow remained elevated but attenuated relative to PFP-1, in all watersheds except East Twin Creek. For comparison, Kinoshita and Hogue (2015) concluded that between 2004 and 2013, annual pre-fire low streamflow increased by 1,090% and 120%, while our results estimate streamflow increased by 91% and 152%, in Devil Canyon Creek and City Creek, respectively. While our results for City Creek align closely with Kinoshita and Hogue (2015), we estimate a much smaller increase in low flow at Devil Canyon Creek, which is partly related to Ages' overestimation of zero-flow and low streamflow.

Changes in streamflow were generally consistent with the areal extent of the burn. The two watersheds with the highest percentage of moderate to high severity burn area, Devil Canyon Creek and City Creek, also experienced the greatest increases in streamflow. Devil Canyon Creek had more percent area burned and more moderate to high severity burn than City Creek, but City Creek had greater percent increases in baseflow and streamflow compared to the unburned condition. While Devil Canyon Creek, City Creek, and Plunge Creek experienced consistent increases in streamflow relative to the unburned conditions, East Twin Creek did not clearly demonstrate this behavior (Figure 15). At first, this inconsistency is perplexing considering that, from October 2002 to November 2003, burn patterns in East Twin Creek were similar to City Creek. However, East Twin Creek is the only San Bernardino watershed that

experienced a major fire after 1970, with 83% of East Twin Creek burning in the 1980 Panorama Fire (Table A.1). Considering that Devil Canyon Creek, City Creek, and Plunge Creek continue to have elevated streamflow 18 years after the Old Fire, it is likely that the calibration period for East Twin Creek (1994-2002, which is 14 to 22 years after the Panorama Fire) coincided with a period of recovery from the 1980 Panorama Fire. Therefore, East Twin Creek was likely in the process of recovering from the Panorama Fire during much or all of its "pre-fire" calibration period.

According to NLCD, vegetation had not returned to its pre-fire composition by 2019, which is 16 years after the fire. Between 2001 and 2019, the coverage by evergreens decreased 60%, 71%, 62%, and 43% in Devil Canyon Creek, City Creek, East Twin Creek, and Plunge Creek, respectively. Excluding East Twin Creek, decreases in evergreen coverage align with increases in streamflow for the San Bernardino watersheds, suggesting that the percent decrease in tree coverage may be a predictor of post-fire streamflow change. While changes in LAI and streamflow were inversely related, results indicate that the return to basin-wide pre-fire values of LAI do not correspond to streamflow recovery. For example, while 2011 LAI values at City Creek and Devil Canyon Creek were only 0.7% and 3.4% lower than their respective 2003 pre-fire values, streamflow remained particularly elevated relative to the unburned condition from 2011 to 2016 (Figure 15). Even as LAI consistently exceeded pre-fire values between 2017-2020, streamflow remained elevated.

City Creek and Devil Canyon Creek likely experienced the greatest increases in streamflow because they had the highest percentage of moderate to high severity burns in addition to the greatest percent loss of tree cover. Less than half of Plunge Creek's watershed burned in the Old Fire, but this fraction was still enough to consistently elevate low streamflow

and annual yield throughout both post-fire periods. Although a high percentage of the East Twin Creek watershed also experienced moderate to high severity burns resulting from the Arrowhead and Old Fires, changes in streamflow were attenuated in comparison to the other San Bernardino watersheds, likely because the watershed had not fully recovered from the 1980 Panorama Fire. Based upon this analysis, none of the San Bernardino watersheds had returned to pre-fire streamflow conditions 18 years after the Old Fire.

# 6. CONCLUSIONS

Changes in daily streamflow due to wildfire were estimated in six study watersheds. For each watershed, the Ages model was calibrated for a pre-fire period. The pre-fire calibrated models were then applied to the post-fire periods to simulate daily streamflow for unburned conditions. The isolated effect of the wildfire on streamflow was determined by comparing measured streamflow (burned condition) to simulated streamflow (unburned condition) after fire. The following conclusions can be drawn from this study:

- All six watersheds experienced a prolonged period of increased streamflow in the years following wildfire. The most consistent and largest relative changes in streamflow occurred during periods of low streamflow. However, streamflow increased at all EPs for at least one post-fire period at all watersheds except Lopez Creek, which only experienced an increase in streamflow above 15% EP. A primary mechanism that increases streamflow following fire may be the coupled interaction between vegetation and subsurface water storage. Following fire, the loss of vegetation reduces transpiration rates, which partitions additional subsurface water into baseflow and interflow, which then increases the percentage of precipitation that becomes streamflow. In certain cases, subsurface water content may become high enough to consistently reduce infiltration capacity, resulting in elevated storm runoff.
- Only one watershed, Lopez Creek, experienced a prolonged period of decreased streamflow. This decrease followed a 6-year-long increase in streamflow and persisted for 6 years. This result indicates that post-fire streamflow does not always remain constant or increase but can decrease for a period as well (perhaps in response to rapid growth new vegetation after fire).

- North Eagle Creek continued to demonstrate elevated streamflow 9 years post-fire, but showed signs of recovery, indicated by the shift from perennial to intermittent streamflow 4 years post-fire. Similarly, all four San Bernardino watersheds continued to display elevated levels of streamflow 18 years post-fire. Devil Canyon Creek, City Creek, and Plunge Creek showed signs of recovery, demonstrated by smaller changes in streamflow relative to unburned conditions 13 to 18 years post-fire. Only one watershed, Lopez Creek, demonstrated a return to pre-fire streamflow behavior during the post-fire study periods (streamflow very similar to the unburned condition was reestablished 12 years post-fire).
- The largest changes in streamflow may not occur until multiple years after a fire. This is evidenced by the limited changes in streamflow measured at North Eagle Creek throughout its first post-fire period (1.9 years). It is possible that the delay in elevated streamflow occurred because of initially high subsurface water storage availability, which gradually decreased due to reduced transpiration.
- Previous fire history influences the effect of subsequent wildfires on streamflow. If a watershed is actively recovering from a previous wildfire, effects of the subsequent wildfire will likely be attenuated. This is supported by the small increase in post-fire streamflow at East Twin Creek when compared to the increases seen at the three other San Bernardino watersheds.
- Weather appears to influence post-fire changes in streamflow behavior. The largest percent increases in streamflow coincided with relatively dry periods, while the smallest percent increases coincided with relatively wet periods. As an example, some of the largest increases in streamflow at the San Bernardino watersheds occurred in the dry

years (i.e., 2007 and 2012-2015) while some of the smallest changes occurred during the wet years (2005, 2008, 2010). This behavior may occur because slight increases in water available for streamflow (due to a reduction in transpiration) have a larger impact on streamflow during periods of limited water. Furthermore, it is hypothesized that the decrease in streamflow at Lopez Creek during PFP-2 was a result of above-average precipitation which produced temporarily elevated biomass and transpiration rates.

Future research should focus on better linking the residual (i.e., the isolated effect of fire on streamflow) with the associated changes in hydrologic processes due to fire. Comparing the differences between a selected number of calibrated pre- and post-fire parameters (similar to Mankin et al., 2022) could identify the hydrologic processes and characteristics that are most responsible for changes in streamflow due to wildfire and test a number of the interpretations presented in this research. Increasing the temporal resolution (where subdaily data are available) to better match the timescale of rainfall-runoff processes could better capture some of these processes. Additionally, this study only explored the effects of three wildfires on streamflow; because wildfires and watersheds vary widely, future work should use this (or similar) methodology at additional sites to determine how the combination of different variables (e.g., burn severity, watershed characteristics, climate, etc.) affect post-fire streamflow.

## 7. TABLES AND FIGURES

Table 1. Study watershed characteristics, fire characteristics (MTBS, 2022), and pre-fire and post-fire analysis periods. [Mod-High Severity= Fraction of watershed having moderate to high burn severity, PFP=post-fire period. Values of forest, shrub/scrub, and herbaceous spatial coverage indicate pre-fire condition and 1-year post-fire (in parentheses).]

| | **N Eagle Ck** | **Lopez Ck** | **Devil Cyn Ck** | **City Ck** | **E Twin Ck** | **Plunge Ck** |
|---|---|---|---|---|---|---|
| Watershed Area | 13.9 $km^2$ | 54.0 $km^2$ | 14.5 $km^2$ | 51.5 $km^2$ | 23.6 $km^2$ | 43.4 $km^2$ |
| Mean Slope | 48% | 52% | 50% | 47% | 49% | 44% |
| Elevation Range | 2330-3250 m | 180-870 m | 630-1650 m | 440-1970 m | 490-1870 m | 520-2000m |
| Local Soil and Thickness | gravelly clay loam, 0.75 m | clay loam with gravel, 0.4-1.3 m | gravelly sandy loam, 0.9 m | gravelly sandy loam, 0.4-1.5 m | gravelly sandy loam, 0.4-1.5 m | gravelly sandy loam, 0.4-1.5 m |
| Forest | 94% (58%) | -- | 45% (13%) | 43% (9%) | 32% (8%) | 30% (26%) |
| Shrub/Scrub | 3% (6%) | -- | 48% (4%) | 50% (9%) | 61% (12%) | 52% (27%) |
| Herbaceous | 2% (34%) | -- | 0% (76%) | 2% (76%) | 1% (73%) | 9% (38%) |
| **Primary Fire** | **2003 Little Bear** | **1985 Las Pilitas** | **2003 Old** | **2003 Old** | **2003 Old** | **2003 Old** |
| Burned Area | 93% | 100% | 96% | 84% | 94% | 49% |
| Mod-High Severity | 34% | 53% | 71% | 58% | 43% | 21% |
| Other Notable Fire | -- | -- | -- | 2003 Bridge | 2002 Arrowhead | 2007 Slide |
| Other Burned Area | -- | -- | -- | 10% | 43% | 24% |
| Pre-fire Start (yrs) | 9/6/07 (4.7) | 2/1/81 (4.4) | 10/1/94 (9.1) | 10/1/94 (8.9) | 10/1/94 (7.7) | 10/1/94 (9.1) |
| Fire Start | 6/4/12 | 7/1/85 | 10/25/03 | 9/5/03 | 5/1/02 | 10/25/03 |
| PFP-1 Start (yrs) | 7/31/12 (1.9) | 7/16/85 (5.6) | 11/3/03 (13.1) | 11/3/03 (13.1) | 11/3/03 (13.1) | 11/3/03 (13.1) |
| PFP-2 Start (yrs) | 7/1/14 (1.9) | 2/28/91 (5.8) | 12/21/16 (5.0) | 12/21/16 (5.0) | 12/21/16 (5.0) | 12/21/16 (5.0) |
| PFP-3 Start (yrs) | 6/1/16 (5.6) | 12/31/96 (14.0) | -- | -- | -- | -- |
| Study Period End (total PFP yrs) | 12/31/21 (9.4) | 12/31/10 (25.5) | 12/31/21 (18.2) | 12/31/21 (18.2) | 12/31/21 (18.2) | 12/31/21 (18.2) |

Table 2. Modeling periods and performance statistics for each watershed. Performance statistics are organized as values from the split sample analysis and final calibration (in parentheses). [NSE=Nash-Sutcliffe efficiency, NSE-Log=NSE calculated on the log of streamflow, KGE=Kling-Gupta efficiency, Calib.=Calibration.]

| | **N Eagle Ck** | **Lopez Ck** | **Devil Cyn Ck** | **City Ck** | **E Twin Ck** | **Plunge Ck** |
|---|---|---|---|---|---|---|
| **Warmup Start** (yrs) | 10/1/05 (1.9) | 1/1/81 (0.1) | 10/1/92 (2.0) | 10/1/92 (2.0) | 10/1/92 (2.0) | 10/1/92 (2.0) |
| **Split Sample Start** | 9/6/07 | 2/1/81 | 10/1/94 | 10/1/94 | 10/1/94 | 10/1/94 |
| Split 1 End (yrs) | 12/31/09 (2.3) | 12/31/82 (1.9) | 12/31/99 (5.3) | 12/31/99 (5.3) | 12/31/99 (5.3) | 12/31/99 (5.3) |
| NSE | 0.944 (0.916) | 0.756 (0.716) | 0.859 (0.844) | 0.863 (0.855) | 0.904 (0.884) | 0.890 (0.889) |
| NSE-Log | 0.467 (0.428) | 0.605 (0.596) | 0.429 (0.417) | 0.546 (0.548) | 0.511 (0.440) | 0.443 (0.406) |
| KGE | 0.972 (0.816) | 0.846 (0.756) | 0.926 (0.910) | 0.930 (0.922) | 0.949 (0.882) | 0.944 (0.940) |
| Bias | 0.8% (17.9%) | 3.6% (6.6%) | -1.9% (-2.2%) | -0.1% (2.3%) | -1.7% (-6.1%) | 0.2% (2.0%) |
| Split 2 End (yrs) | 6/3/12 (2.4) | 6/30/85 (2.5) | 10/24/03 (3.8) | 9/4/03 (3.7) | 5/30/02 (2.4) | 10/24/03 (3.8) |
| NSE | 0.388 (0.880) | 0.515 (0.657) | 0.726 (0.730) | 0.563 (0.665) | 0.638 (0.703) | 0.562 (0.582) |
| NSE-Log | 0.410 (0.645) | 0.549 (0.656) | 0.198 (0.222) | 0.391 (0.451) | 0.205 (0.274) | 0.355 (0.371) |
| KGE | 0.292 (0.836) | 0.750 (0.829) | 0.850 (0.807) | 0.650 (0.772) | 0.618 (0.738) | 0.741 (0.739) |
| Bias | -52.5% (12.9%) | -7.2% (-2.5%) | -6.5% (-12.3%) | -24.6% (-15.7%) | 30.2% (26.3%) | -9.1% (-10.0%) |
| **Final Calib. Start** | 9/6/07 | 2/1/81 | 10/1/94 | 10/1/94 | 10/1/94 | 10/1/94 |
| Final Calib. End (yrs) | 6/3/12 (4.7) | 6/30/85 (4.4) | 10/24/03 (9.1) | 9/4/03 (8.9) | 5/30/02 (7.7) | 10/24/03 (9.1) |
| NSE | 0.750 (0.904) | 0.612 (0.684) | 0.862 (0.851) | 0.860 (0.855) | 0.907 (0.888) | 0.881 (0.880) |
| NSE-Log | 0.435 (0.553) | 0.595 (0.649) | 0.362 (0.367) | 0.511 (0.541) | 0.517 (0.509) | 0.416 (0.396) |
| KGE | 0.644 (0.951) | 0.806 (0.822) | 0.926 (0.916) | 0.920 (0.926) | 0.953 (0.931) | 0.934 (0.939) |
| Bias | -31.6% (-0.8%) | -3.9% (0.3%) | -2.7% (4.0%) | -3.6% (-0.3%) | 1.4% (-3.0%) | -1.4% (-0.1%) |

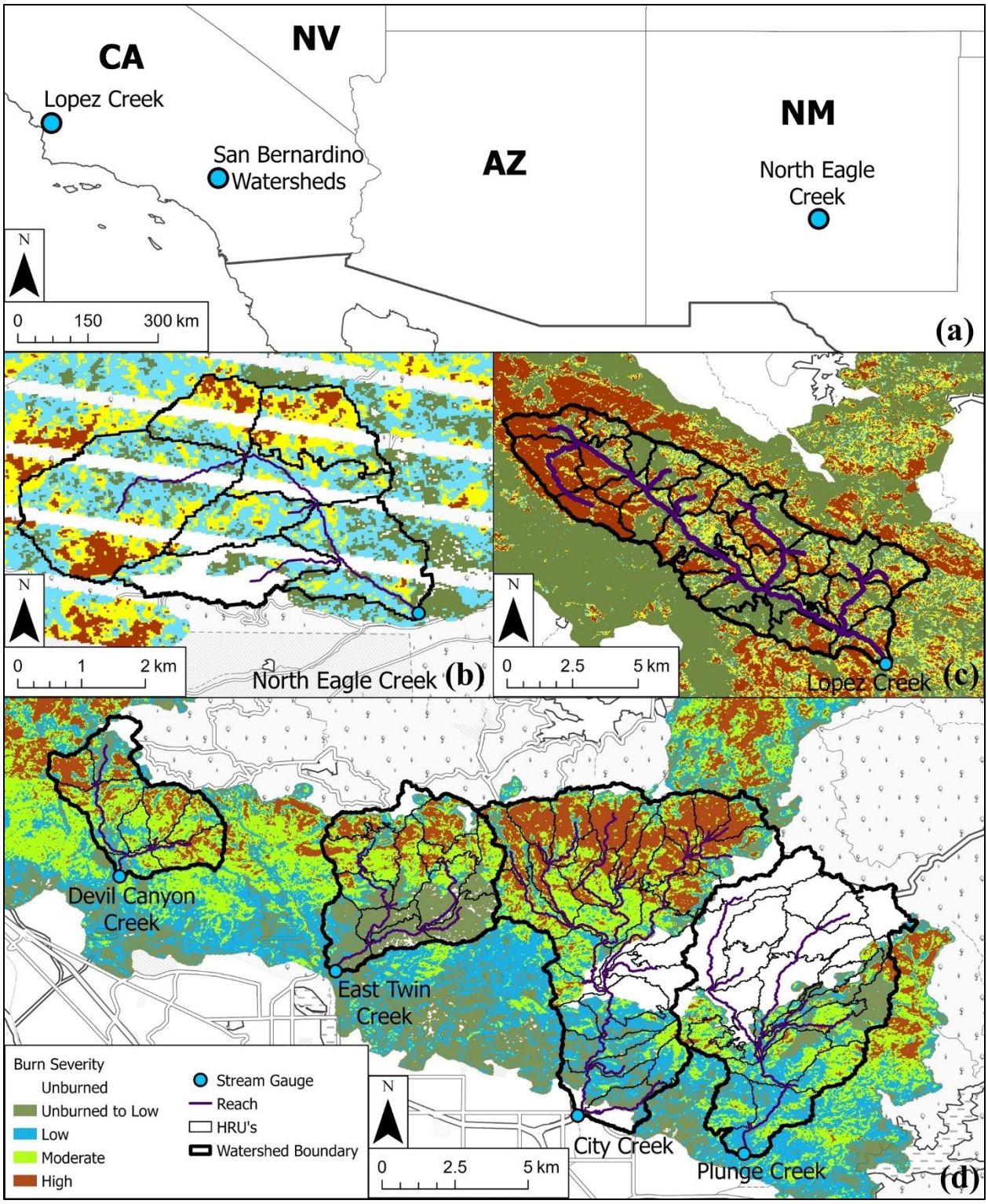


Figure 1. Study watersheds including: (a) location map, (b) North Eagle Creek, (c) Lopez Creek, and (d) San Bernardino watersheds

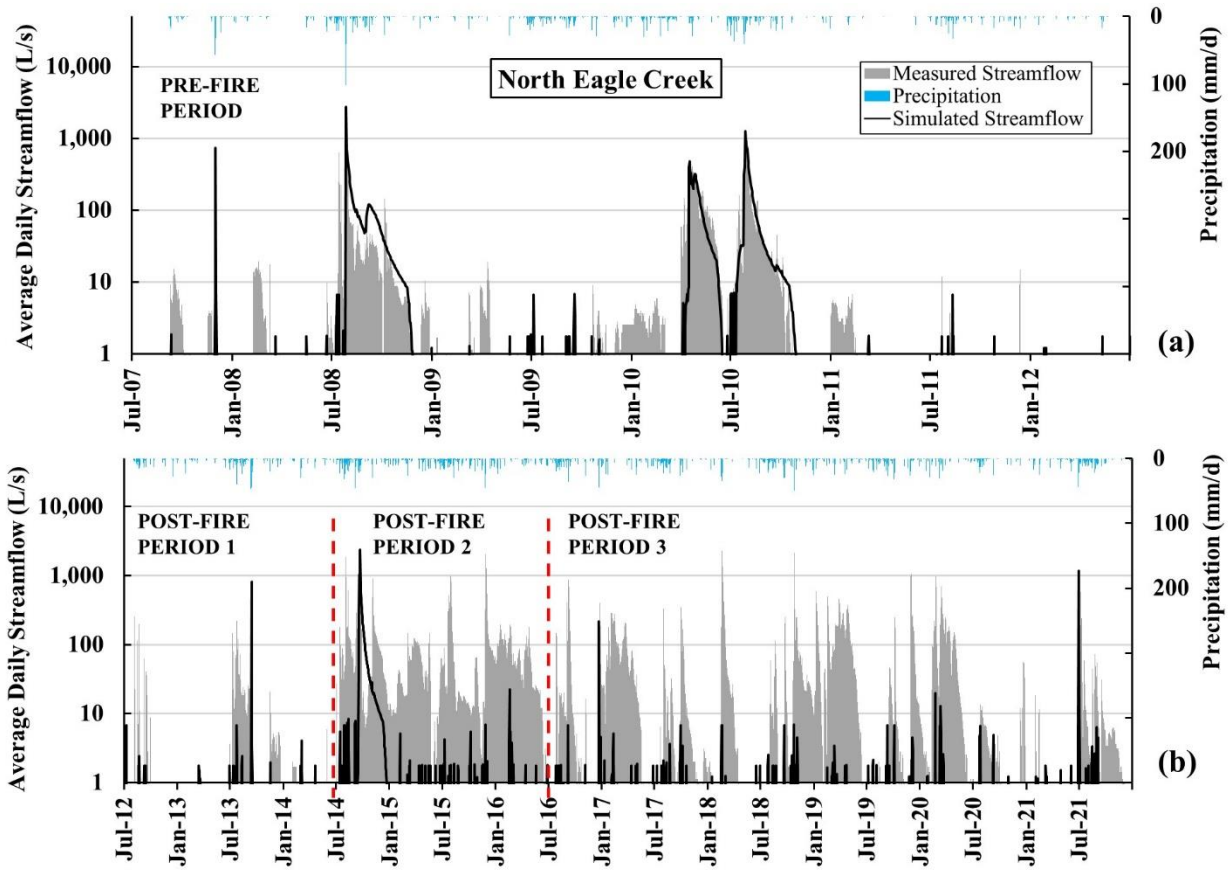


Figure 2. Measured and simulated hydrographs for North Eagle Creek for the (a) pre-fire and (b) post-fire periods. The Little Bear Fire occurred between June 4 and July 30, 2012. In the post-fire periods, measured streamflow and simulated streamflow represent burned and unburned conditions, respectively.

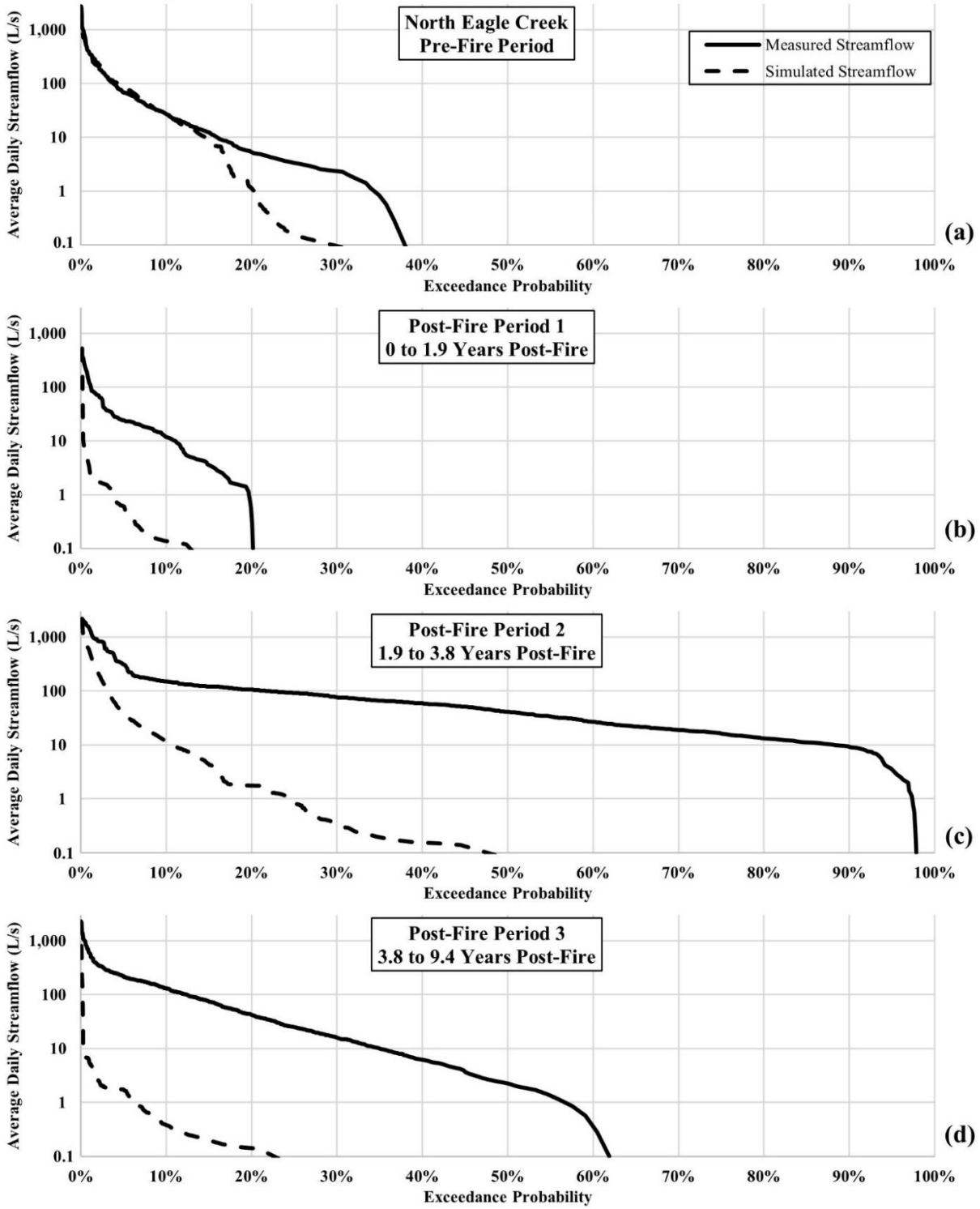


Figure 3. Flow duration curves for North Eagle Creek for the (a) pre-fire period, (b) post-fire period 1, (c) post-fire period 2, and (d) post-fire period 3. In the post-fire periods, measured streamflow and simulated streamflow represent burned and unburned conditions, respectively. Note that streamflow less than or equal to 0.1 L/s is not shown.

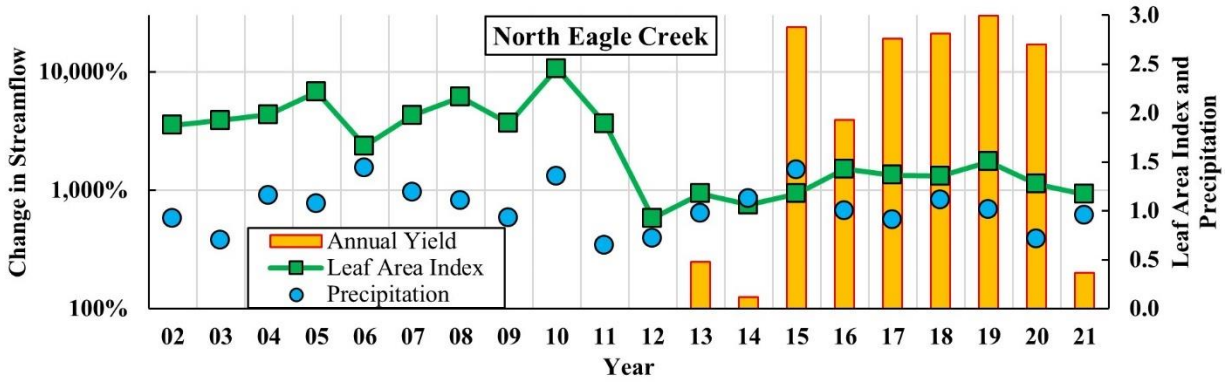


Figure 4. Annual change in streamflow, leaf area index, and precipitation at North Eagle Creek. Note that precipitation is expressed as the ratio of annual precipitation of the year shown divided by the average precipitation throughout the study period.

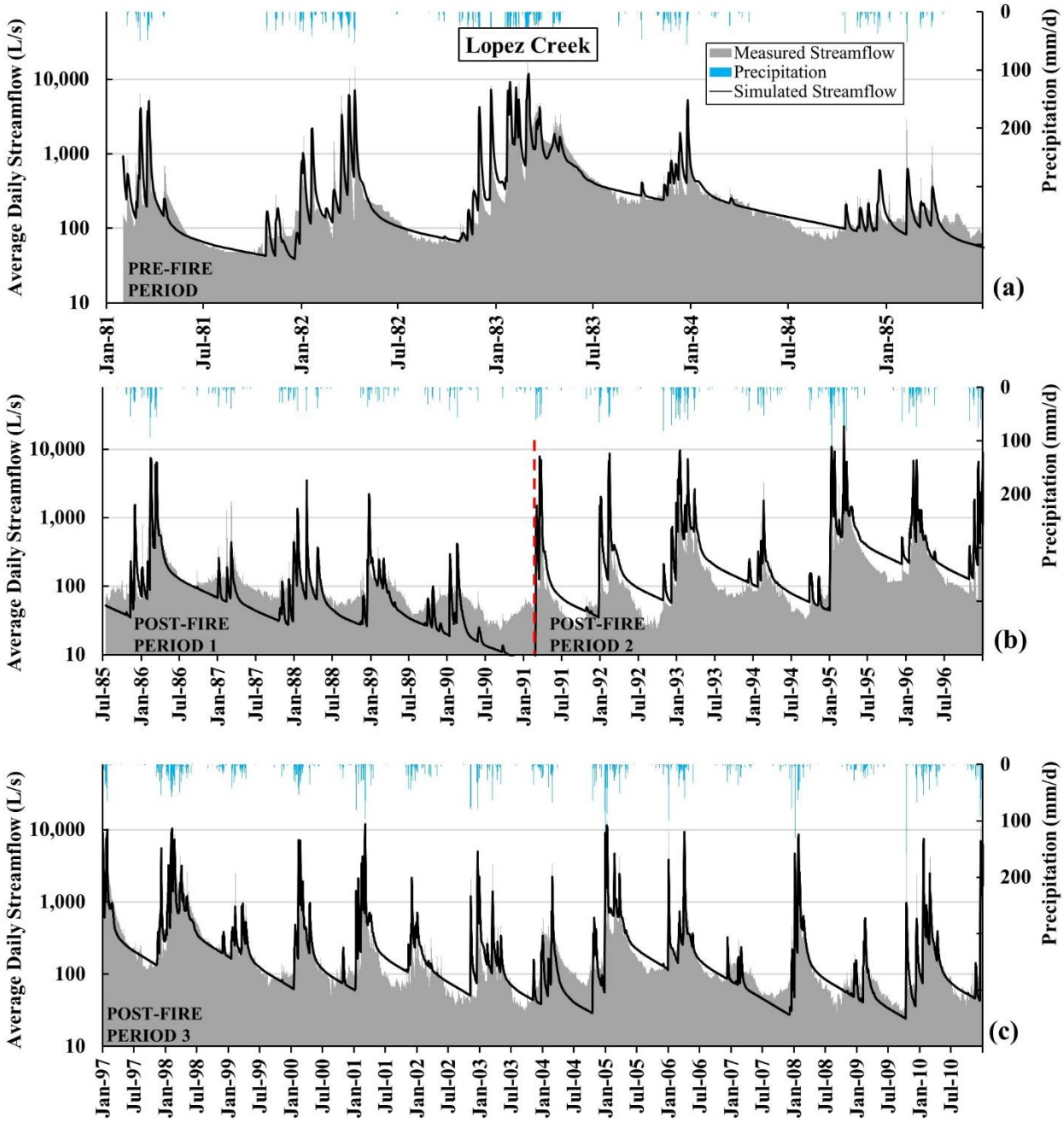


Figure 5. Measured and simulated hydrographs for Lopez Creek for the (a) pre-fire period, (b) post-fire periods 1 and 2, and (c) post-fire period 3. The Las Pilitas Fire occurred between July 1 and July 15, 1985. In the post-fire periods, measured streamflow and simulated streamflow represent burned and unburned conditions, respectively.

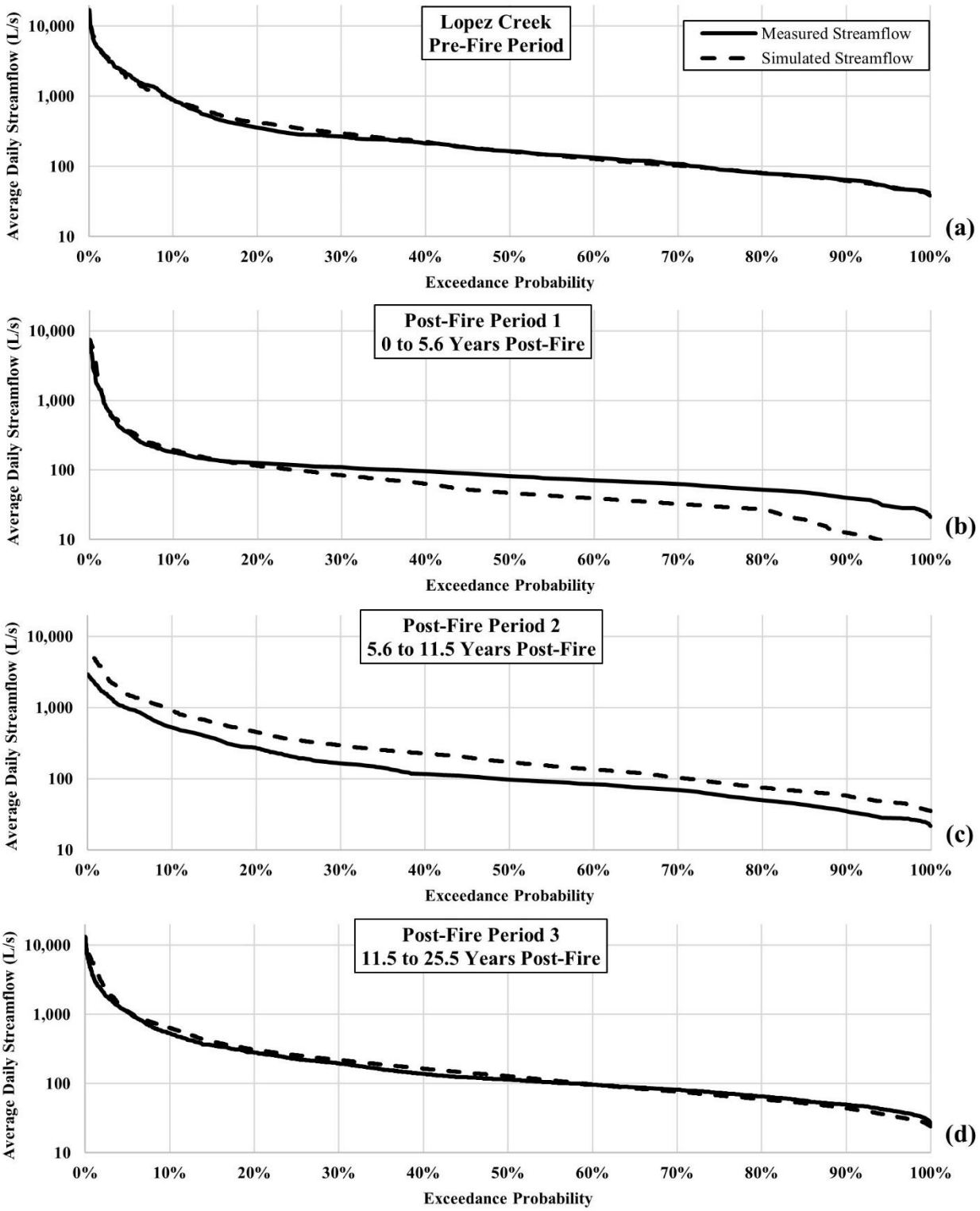


Figure 6. Flow duration curves for Lopez Creek for the (a) pre-fire period, (b) post-fire period 1, (c) post-fire period 2, and (d) post-fire period 3. In the post-fire periods, measured streamflow and simulated streamflow represent burned and unburned conditions, respectively. Note that streamflow less than or equal to 10 L/s is not shown.

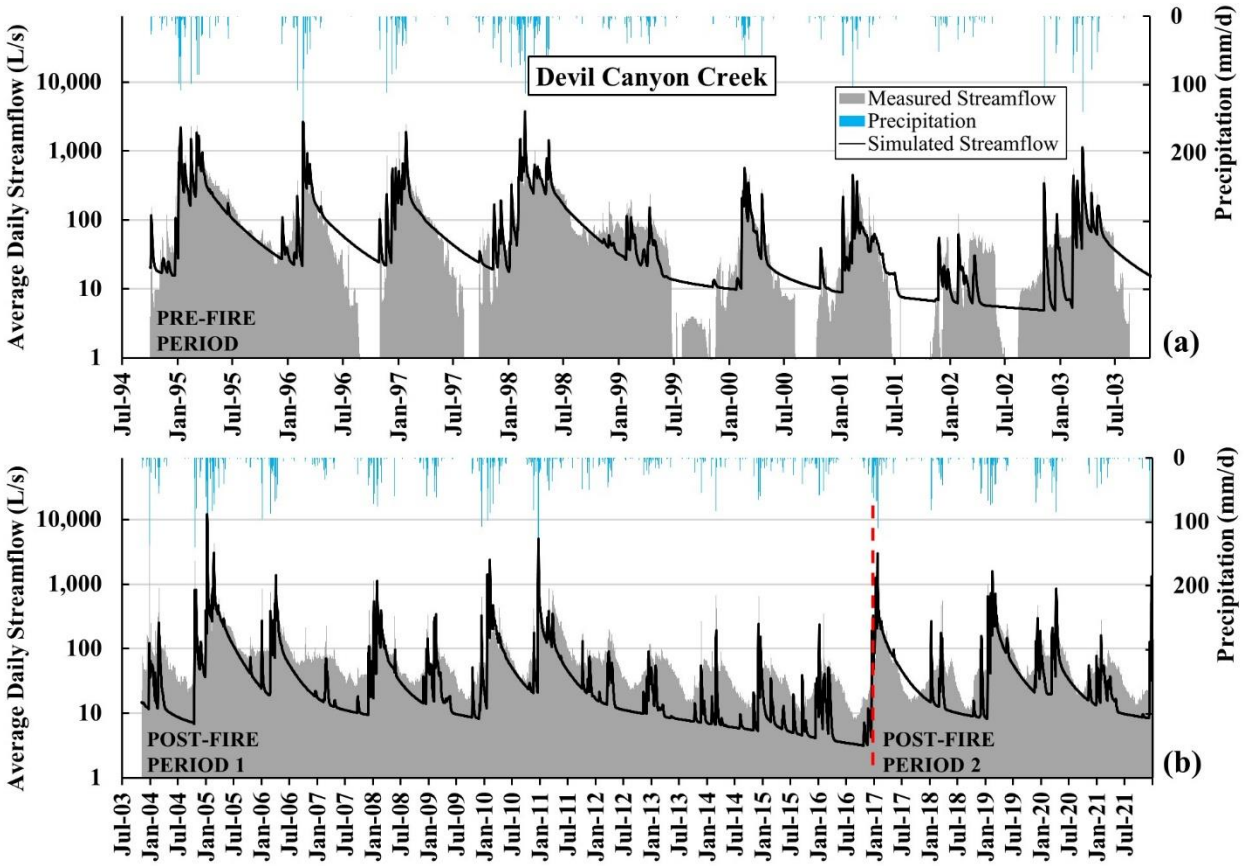


Figure 7. Measured and simulated hydrographs for Devil Canyon Creek for the (a) pre-fire and (b) post-fire periods. The Old Fire occurred between October 25 and November 2, 2003. In the post-fire periods, measured streamflow and simulated streamflow represent burned and unburned conditions, respectively.

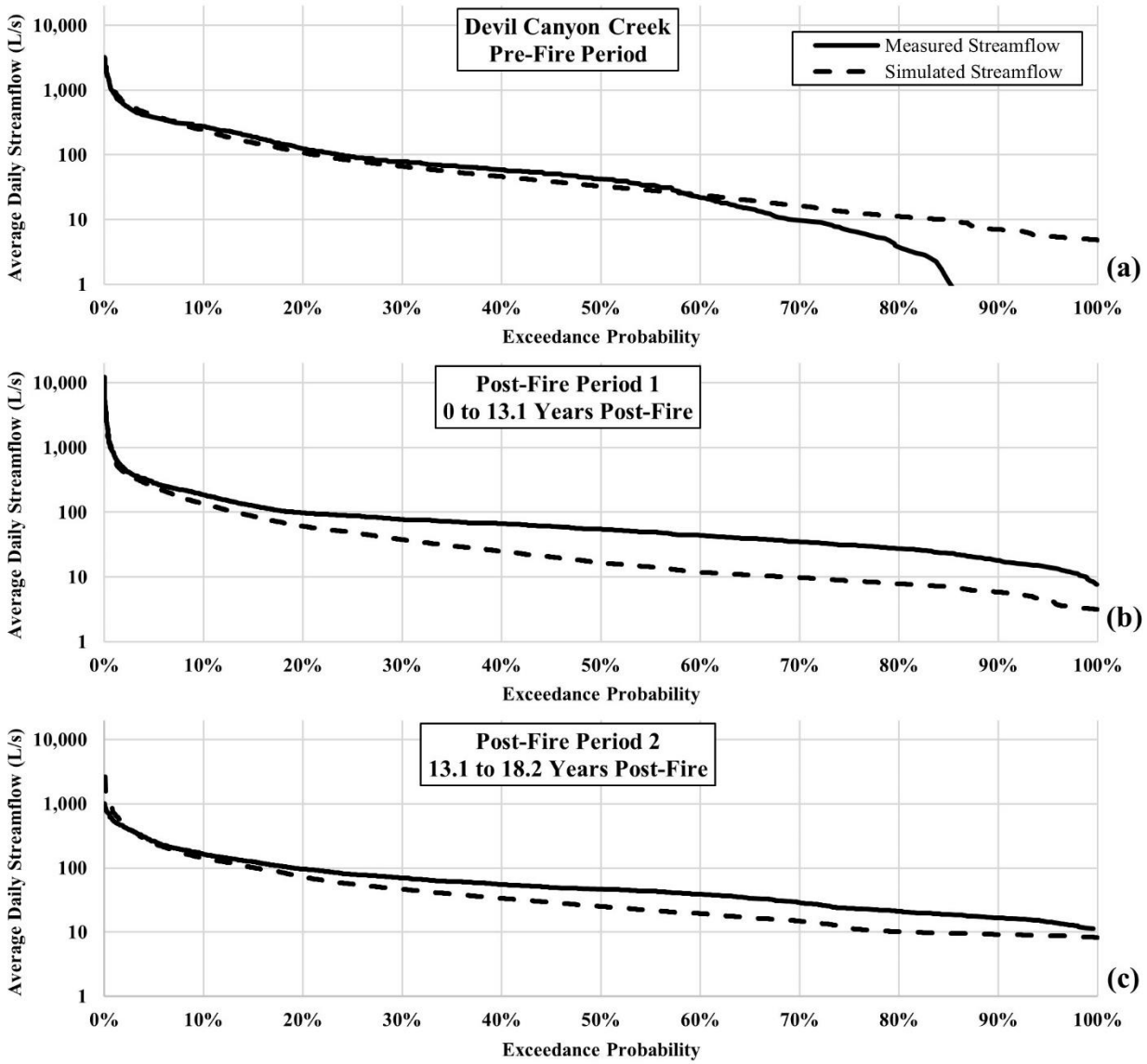


Figure 8. Flow duration curves for Devil Canyon Creek for the (a) pre-fire period, (b) post-fire period 1, and (c) post-fire period 2. In the post-fire periods, measured streamflow and simulated streamflow represent burned and unburned conditions, respectively. Note that streamflow less than or equal to 1 L/s is not shown.

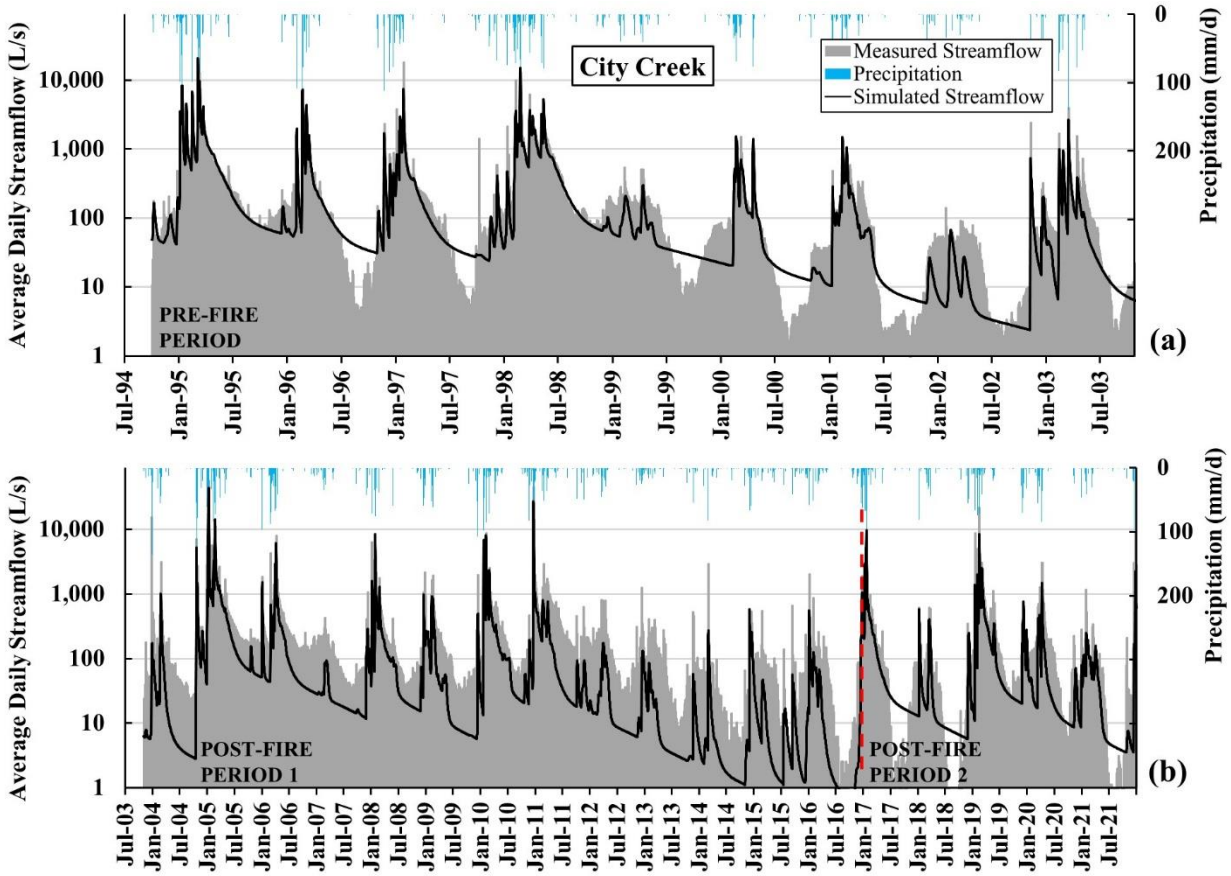


Figure 9. Measured and simulated hydrographs for City Creek for the (a) pre-fire period and (b) post-fire periods. The Old Fire occurred between October 25 and November 2, 2003. In the post-fire periods, measured streamflow and simulated streamflow represent burned and unburned conditions, respectively.

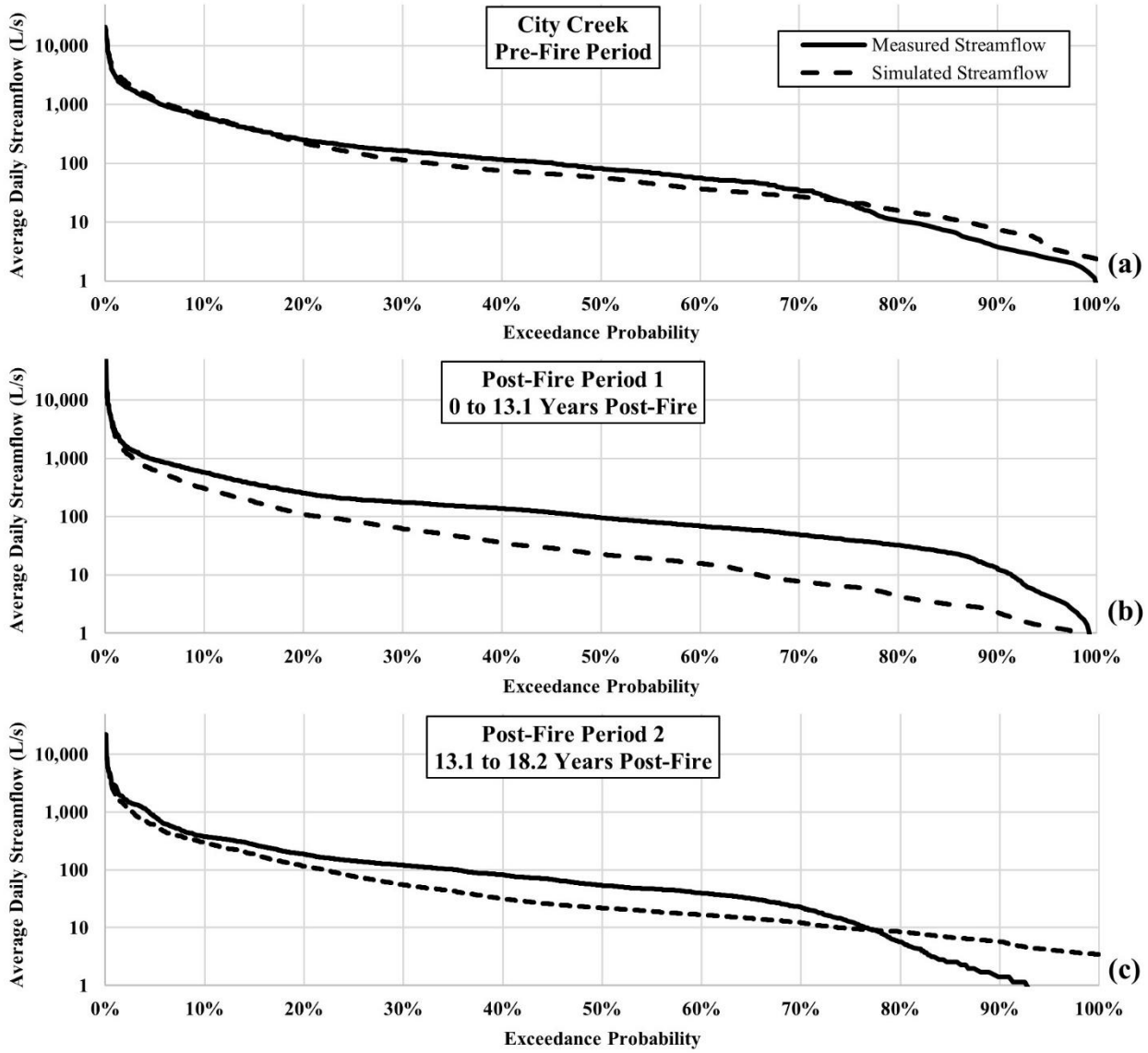


Figure 10. Flow duration curves for City Creek for the (a) pre-fire period, (b) post-fire period 1, and (c) post-fire period 2. In the post-fire periods, measured streamflow and simulated streamflow represent burned and unburned conditions, respectively. Note that streamflow less than or equal to 1 L/s is not shown.

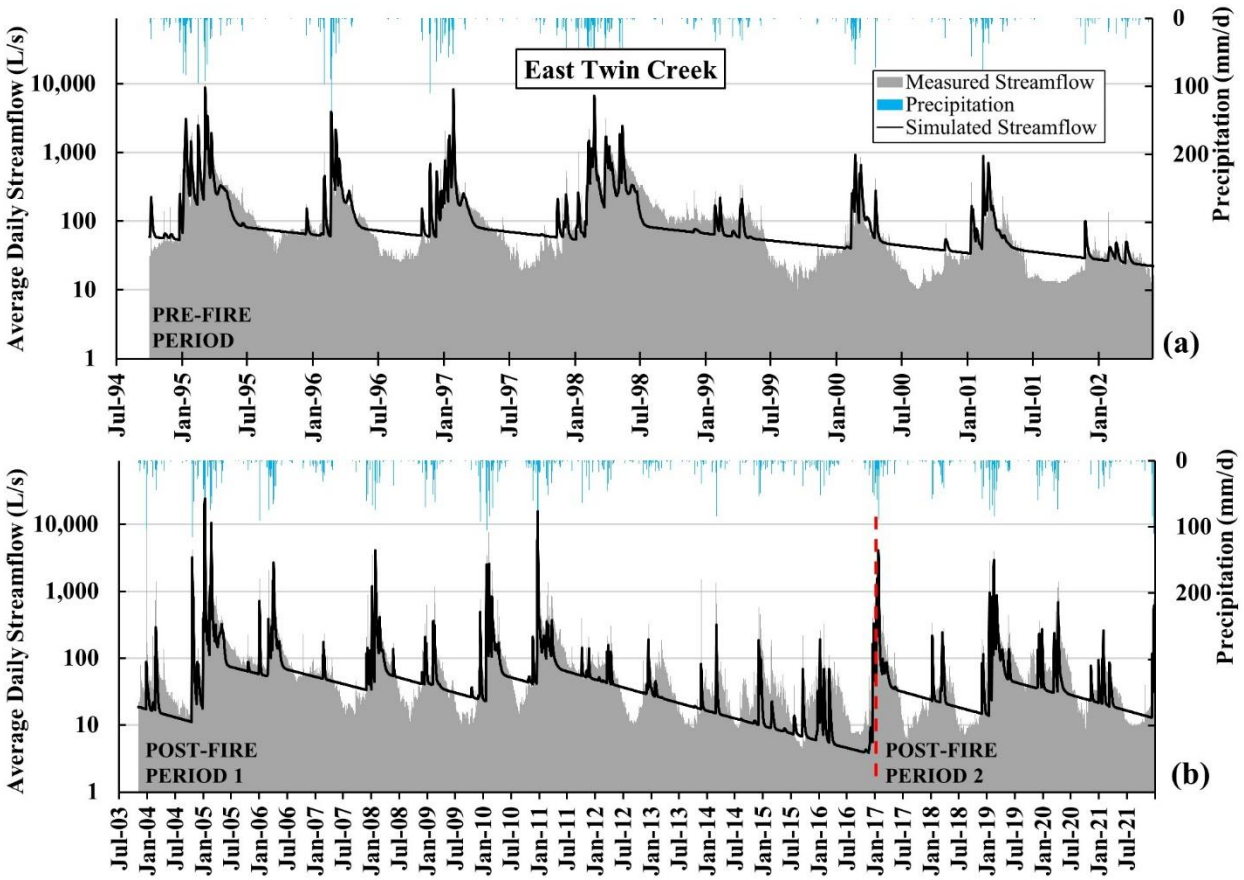


Figure 11. Measured and simulated hydrographs for East Twin Creek for the (a) pre-fire and (b) post-fire periods. The Old Fire occurred between October 25 and November 2, 2003. In the post-fire periods, measured streamflow and simulated streamflow represent burned and unburned conditions, respectively.

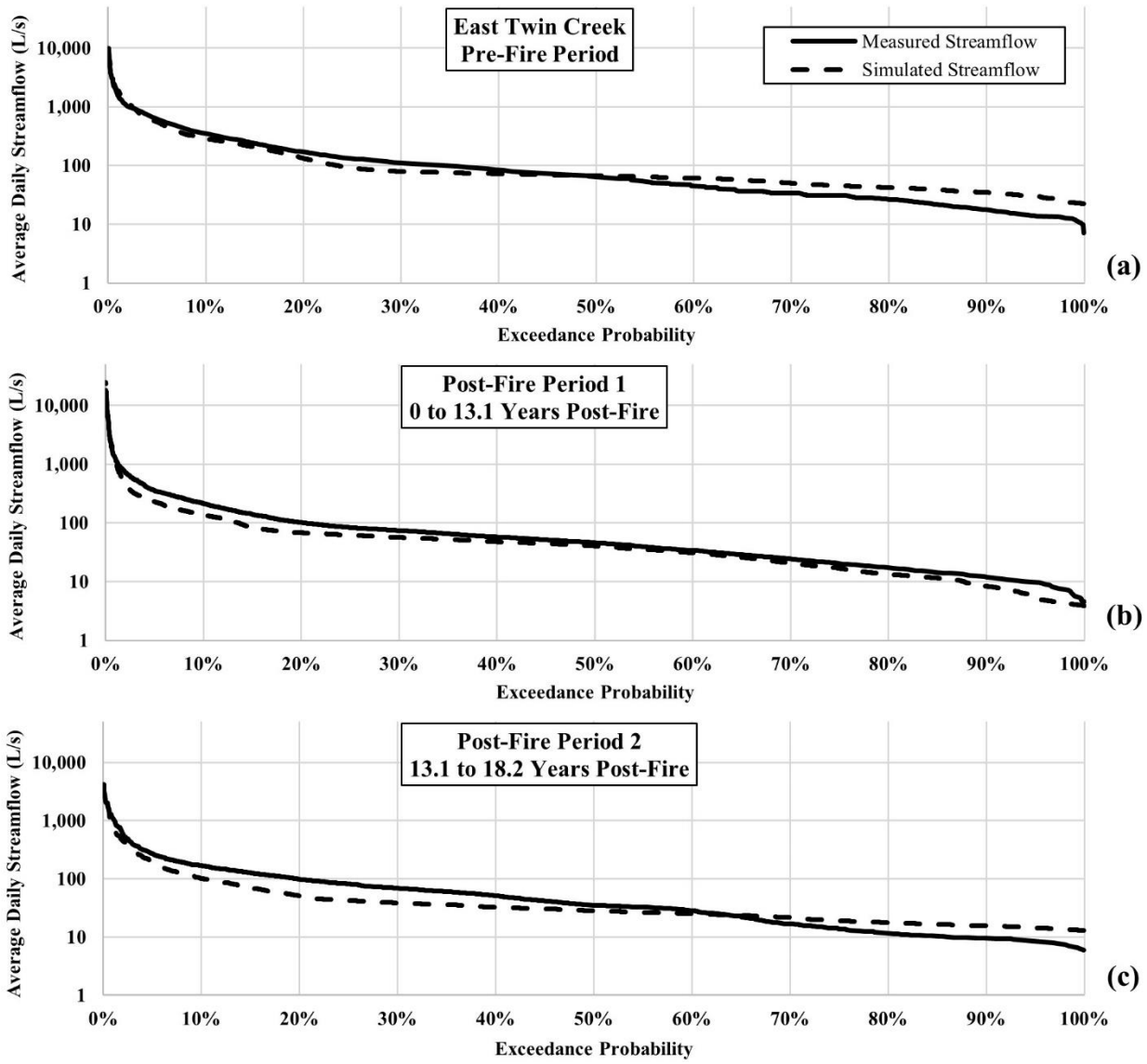


Figure 12. Flow duration curves for East Twin Creek for the (a) pre-fire period, (b) post-fire period 1, and (c) post-fire period 2. In the post-fire periods, measured streamflow and simulated streamflow represent burned and unburned conditions, respectively.

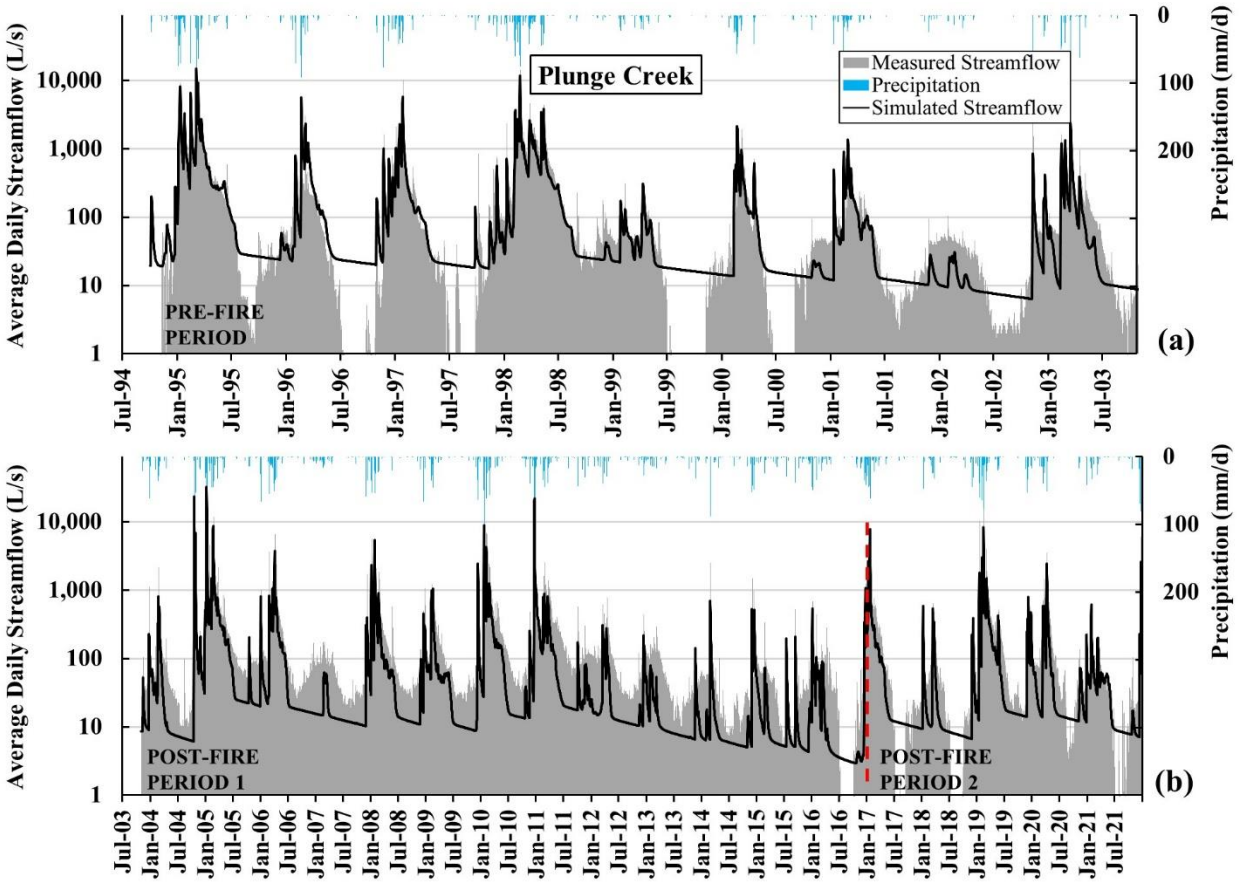


Figure 13. Measured and simulated hydrographs for Plunge Creek for the (a) pre-fire and (b) post-fire periods. The Old Fire occurred between October 25 and November 2, 2003. In the post-fire periods, measured streamflow and simulated streamflow represent burned and unburned conditions, respectively.

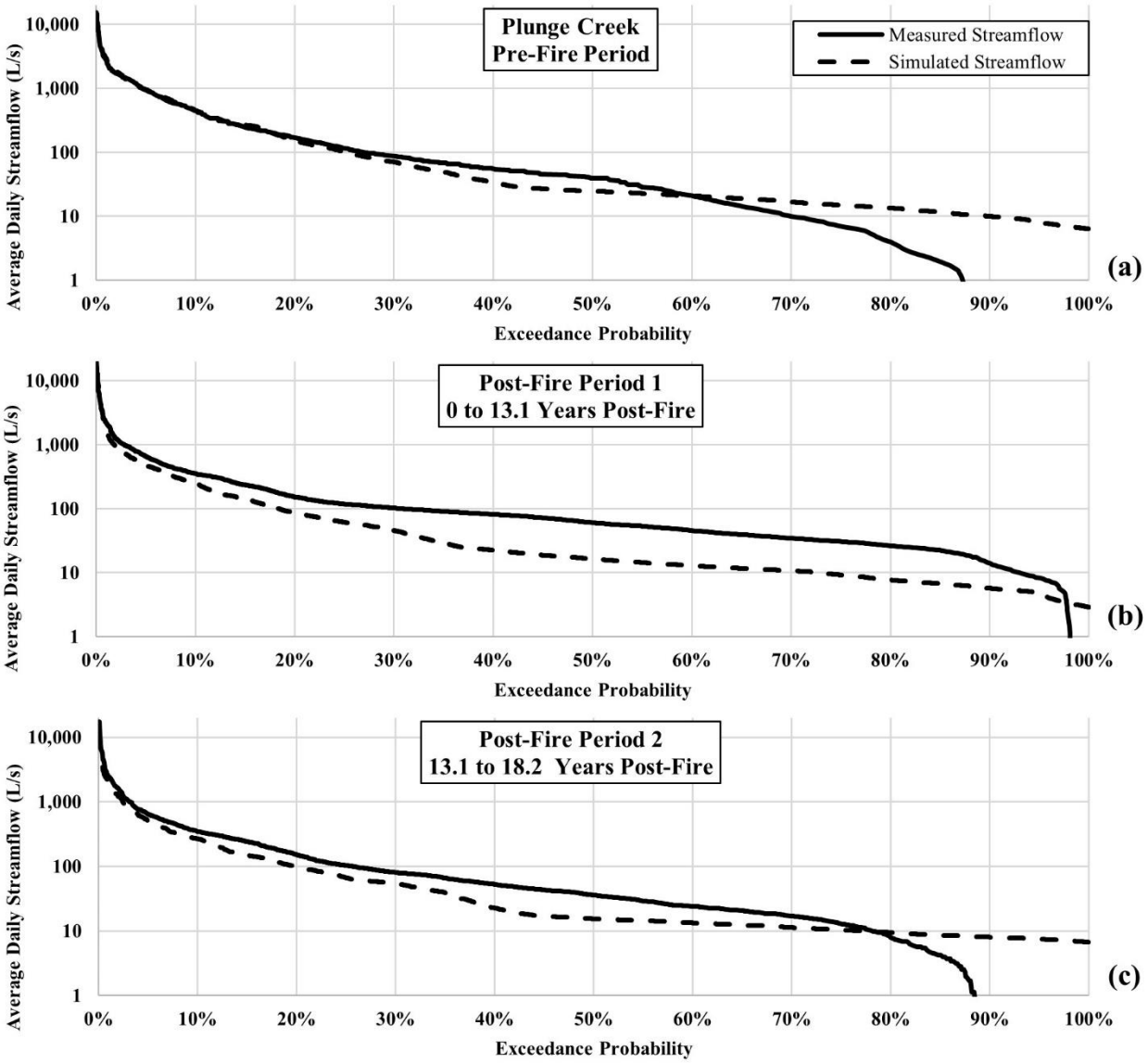


Figure 14. Flow duration curves for Plunge Creek for the (a) pre-fire period, (b) post-fire period 1, and (c) post-fire period 2. In the post-fire periods, measured streamflow and simulated streamflow represent burned and unburned conditions, respectively. Note that streamflow less than or equal to 1 L/s is not shown.

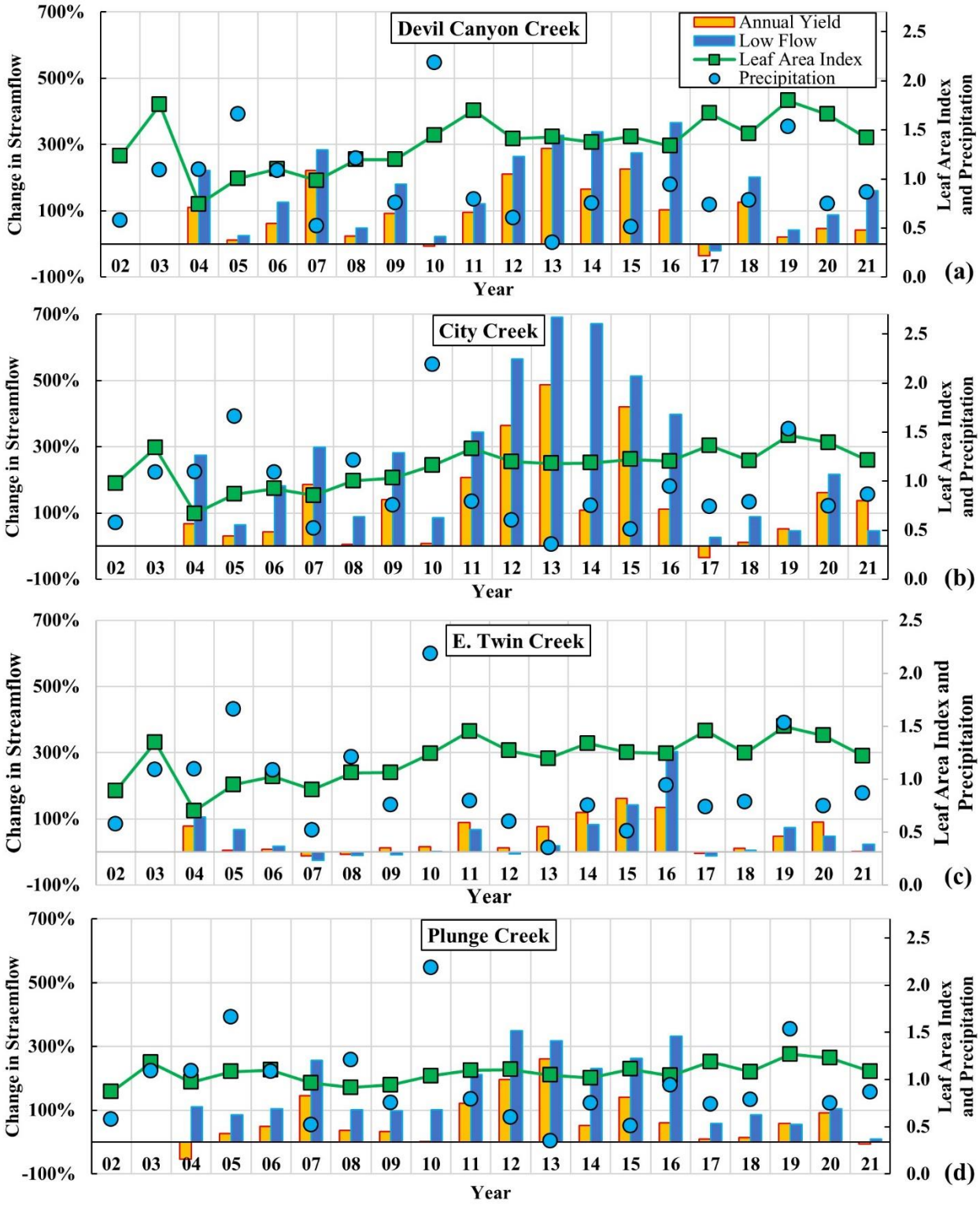


Figure 15. Annual change in streamflow, leaf area index, and precipitation for the San Bernadino watersheds. Note that precipitation is expressed as the ratio of annual precipitation of year 'x' divided by the average precipitation throughout the study period.

REFERENCES


Abatzoglou, J. T. (2013). Development of gridded surface meteorological data for ecological applications and modelling. *International Journal of Climatology*, *33*(1), 121–131. https://doi.org/10.1002/joc.3413

Abatzoglou, J. T., & Kolden, C. A. (2013). Relationships between climate and macroscale area burned in the western United States. *International Journal of Wildland Fire*, *22*(7), 1003. https://doi.org/10.1071/WF13019

Abatzoglou, J. T., & Williams, A. P. (2016). Impact of anthropogenic climate change on wildfire across western US forests. *Proceedings of the National Academy of Sciences*, *113*(42), 11770–11775. https://doi.org/10.1073/pnas.1607171113

Abatzoglou, J. T., Juang, C. S., Williams, A. P., Kolden, C. A., & Westerling, A. L. (2021). Increasing Synchronous Fire Danger in Forests of the Western United States. *Geophysical Research Letters*, *48*(2). https://doi.org/10.1029/2020GL091377

Andreassian, V. (2004). Waters and forests: from historical controversy to scientific debate. *Journal of Hydrology.* 291, 1-27. https://doi.org/10.1016/j.jhydrol.2003.12.015

Ascough, J. C., David, O., Krause, P., Heathman, G. C., Kralisch, S., Larose, M., Ahuja, L. R., & Kipka, H. (2012). Development and Application of a Modular Watershed-Scale Hydrologic Model Using the Object Modeling System: Runoff Response Evaluation. *Transactions of the ASABE*, *55*(1), 117–135. https://doi.org/10.13031/2013.41260

Barnard, D. M., Green, T. R., Mankin, K. R., DeJonge, K. C., Rhoades, C. C., Kampf, S. K., Giovando, J., Wilkins, M. J., Mahood, A. L., Sears, M. G., Comas, L. H., Gleason, S. M., Zhang, H., Fassnacht, S. R., Harmel, R. D., & Altenhofen, J. (2023). Wildfire and climate change amplify knowledge gaps linking mountain source-water systems and agricultural water supply in the western United States. *Agricultural Water Management*, 286, p.108377. https://doi.org/10.1016/j.agwat.2023.108377

Bart, R. R. (2016). A regional estimate of postfire streamflow change in California. *Water Resources Research*, *52*(2), 1465–1478. https://doi.org/10.1002/2014WR016553

Bart, R., & Hope, A. (2010). Streamflow response to fire in large catchments of a Mediterranean-climate region using paired-catchment experiments. *Journal of Hydrology*, *388*(3–4), 370–378. https://doi.org/10.1016/j.jhydrol.2010.05.016

Bart, R. R., & Tague, C. L. (2017). The impact of wildfire on baseflow recession rates in California. *Hydrological Processes*, *31*(8), 1662–1673. https://doi.org/10.1002/hyp.11141

Best, A., Zhang, L., McMahon, T., Western, A., Vertessy, R. (2003). A Critical Review of Paired Catchment Studies with Reference to Seasonal Flows and Climatic Variability. *CSIRO Land and Water Technical Report 25/03*. http://hdl.handle.net/102.100.100/193160?index=1

Blanc, E., Strzepek, K., Schlosser, A., Jacoby, H., Gueneau, A., Fant, C., Rausch, S., & Reilly, J. (2014). Modeling U.S. water resources under climate change. *Earth's Future*, *2*(4), 197–224. https://doi.org/10.1002/2013EF000214

Blount, K., Ruybal, C. J., Franz, K. J., & Hogue, T. S. (2020). Increased water yield and altered water partitioning follow wildfire in a forested catchment in the western United States. *Ecohydrology*, *13*(1). https://doi.org/10.1002/eco.2170

Brown, T. C., Hobbins, M. T., & Ramirez, J. A. (2008). Spatial Distribution of Water Supply in the Coterminous United States. *JAWRA Journal of the American Water Resources Association*, *44*(6), 1474–1487. https://doi.org/10.1111/j.1752-1688.2008.00252.x

Brown, T. C., Mahat, V., & Ramirez, J. A. (2019). Adaptation to Future Water Shortages in the United States Caused by Population Growth and Climate Change. *Earth's Future*, *7*(3), 219–234. https://doi.org/10.1029/2018EF001091

Burles, K., & Boon, S. (2011). Snowmelt energy balance in a burned forest plot, Crowsnest Pass, Alberta, Canada. *Hydrological Processes*, 25, 3012-3029. https://doi.org/10.1002/hyp.8067

Chavarria, S. B., & Gutzler, D. S. (2018). Observed Changes in Climate and Streamflow in the Upper Rio Grande Basin. *JAWRA Journal of the American Water Resources Association*, *54*(3), 644–659. https://doi.org/10.1111/1752-1688.12640

Clark, M. P., Vogel, R. M., Lamontagne, J. R., Mizukami, N., Knoben, W. J. M., Tang, G., Gharari, S., Freer, J. E., Whitfield, P. H., Shook, K. R., & Papalexiou, S. M. (2021). The Abuse of Popular Performance Metrics in Hydrologic Modeling. *Water Resources Research*, *57*(9), e2020WR029001. https://doi.org/10.1029/2020WR029001

Daly, C., Halbleib, M., Smith, J. I., Gibson, W. P., Doggett, M. K., Taylor, G. H., Curtis, J., & Pasteris, P. P. (2008). Physiographically sensitive mapping of climatological temperature

and precipitation across the conterminous United States. *International Journal of Climatology*, *28*(15), 2031–2064. https://doi.org/10.1002/joc.1688

DeBano, L. F. (2000). The role of fire and soil heating on water repellency in wildland environments: A review. *Journal of Hydrology*, *231–232*, 195–206. https://doi.org/10.1016/S0022-1694(00)00194-3

Eidenshink, J., Schwind, B., Brewer, K., Zhu, Z.-L., Quayle, B., & Howard, S. (2007). A Project for Monitoring Trends in Burn Severity. *Fire Ecology*, *3*(1), 3–21. https://doi.org/10.4996/fireecology.0301003

Foti, R., Ramirez, J. A., & Brown, T. C. (2012). *Vulnerability of U.S. water supply to shortage: A technical document supporting the Forest Service 2010 RPA Assessment* (RMRS-GTR-295; p. RMRS-GTR-295). U.S. Department of Agriculture, Forest Service, Rocky Mountain Research Station. https://doi.org/10.2737/RMRS-GTR-295

Giovando, J., & Niemann, J. D. (2022). Wildfire Impacts on Snowpack Phenology in a Changing Climate Within the Western U.S. *Water Resources Research*, *58*(8). https://doi.org/10.1029/2021WR031569

Goeking, S. A., & Tarboton, D. G. (2020). Forests and Water Yield: A Synthesis of Disturbance Effects on Streamflow and Snowpack in Western Coniferous Forests. *Journal of Forestry*, *118*(2), 172–192. https://doi.org/10.1093/jofore/fvz069

Green, T. R., Erskine, R. H., Coleman, M. L., David, O., Ascough, J. C., & Kipka, H. (2015). The AgroEcoSystem (AgES) Response-Function Model Simulates Layered Soil-Water Dynamics in Semiarid Colorado: Sensitivity and Calibration. *Vadose Zone Journal*, *14*(8), vzj2014.09.0119. https://doi.org/10.2136/vzj2014.09.0119

Hallema, D. W., Sun, G., Caldwell, P. V., Norman, S. P., Cohen, E. C., Liu, Y., Ward, E. J., & McNulty, S. G. (2017). Assessment of wildland fire impacts on watershed annual water yield: Analytical framework and case studies in the United States: Wildland fire impacts on annual water yield: Framework and case studies. *Ecohydrology*, *10*(2), e1794. https://doi.org/10.1002/eco.1794

Harmel, R. D., Baffaut, C., & Douglas-Mankin, K. (2018). Review and Development of ASABE Engineering Practice 621: "Guidelines for Calibrating, Validating, and Evaluating Hydrologic and Water Quality Models." *Transactions of the ASABE*, *61*(4), 1393–1401. https://doi.org/10.13031/trans.12806

Harpold, A. A., Biederman, J. A., Condon, K., Merino, M., Korgaonkar, Y., Nan, T., Sloat, L. L., Ross, M., & Brooks, P. D. (2014). Changes in snow accumulation and ablation following the Las Conchas Forest Fire, New Mexico, USA: Changes in Snow Following Fire. *Ecohydrology*, *7*(2), 440–452. https://doi.org/10.1002/eco.1363

Hay, L.E, Umemoto, M. (2006). Multiple-Objective Stepwise Calibration Using Luca. *U.S. Geological Survey Open-File Report 2006-1323*. https://pubs.er.usgs.gov/publication/ofr20061323

Helvey, J. D. (1980). Effects of a North Central Washington Wildfire on Runoff and Sediment Production. *Journal of the American Water Resources Association*, *16*(4), 627–634. https://doi.org/10.1111/j.1752-1688.1980.tb02441.x

Hoyt, W.G., & Troxell, H.C. (1934). Forests and Stream Flow. *Transactions of American Society of Civil Engineers,* 99 1-30.

Hubbert, K. R., Wohlgemuth, P. M., Beyers, J. L., Narog, M. G., & Gerrard, R. (2012). Post-Fire Soil Water Repellency, Hydrologic Response, and Sediment Yield Compared between Grass-Converted and Chaparral Watersheds. *Fire Ecology*, *8*(2), 143–162. https://doi.org/10.4996/fireecology.0802143

Hurd, B., & Coonrod, J. (2012). Hydro-economic consequences of climate change in the upper Rio Grande. *Climate Research*, *53*(2), 103–118. https://doi.org/10.3354/cr01092

Jin, S., Homer, C., Yang, L., Danielson, P., Dewitz, J., Li, C., Zhu, Z., Xian, G., & Howard, D. (2019). Overall Methodology Design for the United States National Land Cover Database 2016 Products. *Remote Sensing*, *11*(24), 2971. https://doi.org/10.3390/rs11242971

Kelley, S., Koning, D. J., Goff, F., Cikoski, C., Peters, L., & McIntosh, W. (2014). Stratigraphy of the northwestern Sierra Blanca volcanic field. *Geology of the Sacramento Mountains Region*, 197–208. https://doi.org/10.56577/FFC-65.197

Kinoshita, A. M., & Hogue, T. S. (2011). Spatial and temporal controls on post-fire hydrologic recovery in Southern California watersheds. *CATENA*, *87*(2), 240–252. https://doi.org/10.1016/j.catena.2011.06.005

Kinoshita, A. M., & Hogue, T. S. (2015). Increased dry season water yield in burned watersheds in Southern California. *Environmental Research Letters*, *10*(1), 014003. https://doi.org/10.1088/1748-9326/10/1/014003

Kipka, H. Lighthart, N., David, O., Green, T. R., Patterson, D., & Arabi, M. (2019). The enhanced Catchment areas delineation (Cadel) tool for watershed models with spatially explicit routing between simulated areas. Proc. Hydrology Days, March 27-29, 2019, Fort Collins, CO.

Knauf, D. (1980). Die Berechnung des Abflusses 59u seiner Schneedecke. In: Analyse und Berechnung oberirdischer Abfl€usse DVWKSchriften, Bonn, Heft 46.

Krause, P. (2002). Quantifying the impact of land use changed on the water balance of large catchments using the J2000 model. *Physics and Chemistry of the Earth, 27*(9-10), 663-673.

Krause, P., U. Bende-Michl, F. Bäse, M. Fink, W-A. Flügel, and B. Pfennig. 2006. Multiscale investigations in a mesoscalecatchment: Hydrological modelling in the Gera catchment. Adv.Geos. 9: 53-61.

Larsen, I. J., MacDonald, L. H., Brown, E., Rough, D., Welsh, M. J., Pietraszek, J. H., Libohova, Z., Dios Benavides-Solorio, J., & Schaffrath, K. (2009). Causes of Post-Fire Runoff and Erosion: Water Repellency, Cover, or Soil Sealing? *Soil Science Society of America Journal*, *73*(4), 1393–1407. https://doi.org/10.2136/sssaj2007.0432

Mahat, V., Silins, U., & Anderson, A. (2016). Effects of wildfire on the catchment hydrology in southwest Alberta. *CATENA*, *147*, 51–60. https://doi.org/10.1016/j.catena.2016.06.040

Mankin, K.R., & Patel, R. (2023). Wildfire burn severity affects postfire shifts in evapotranspiration in subalpine forests. *Journal of Natural Resources and Agricultural Ecosystems, 1*(1), 1-11. https://doi.org/10.13031/jnrae.15438

Mankin, K. R., Wells, R., Kipka, H., Green, T. R., & Barnard, D. (2022). Hydrologic Effects of Fire in a Sub-Alpine Watershed: AgES Outperforms Previous PRMS Simulations. *Journal of the ASABE*, *65*(4), 751–762. https://doi.org/10.13031/ja.14881

Martin, D. A., & Moody, J. A. (2001). Comparison of soil infiltration rates in burned and unburned mountainous watersheds. *Hydrological Processes*, *15*(15), 2893–2903. https://doi.org/10.1002/hyp.380

Moeser, C. D., & Douglas-Mankin, K. R. (2021). Simulating Hydrologic Effects of Wildfire on a Small Sub-Alpine Watershed in New Mexico, US. *Transactions of the ASABE, 64*(1), 137-150. http://doi.org.10.13031/trans.13938

Monitoring Trends and Burn Severity (MTBS). (2022). *Direct Download*. https://mtbs.gov/direct-download

Moody, J. A., Ebel, B. A., Nyman, P., Martin, D. A., Stoof, C., & McKinley, R. (2016). Relations between soil hydraulic properties and burn severity. *International Journal of Wildland Fire*, *25*(3), 279. https://doi.org/10.1071/WF14062

Morton, D. M., & Miller, F. K. (2006). Geologic Map of the San Bernardino and Santa Ana 30' x 60' Quadrangles, California. *U.S. Geological Survey Open-File Report 2006-1217*.

Myneni, R. B., Hoffman, S., Knyazikhin, Y., Privette, J. L., Glassy, J., Tian, Y., Wang, Y., Song, X., Zhang, Y., Smith, G. R., Lotsch, A., Friedl, M., Morisette, J. T., Votava, P., Nemani, R. R., & Running, S. W. (2002). Global products of vegetation leaf area and fraction absorbed PAR from year one of MODIS data. *Remote Sensing of Environment*, *83*(1–2), 214–231. https://doi.org/10.1016/S0034-4257(02)00074-3

National Aeronautics and Space Administration (NASA). (2022). *Extract Area Sample.*

National Interagency Fire Center (NIFC). (2022). *Data*. https://nifc.hub.arcgis.com/search?q=historic%20fire%20perimeters

Natural Resources Conservation Service (NRCS). (2022a). *SNOTEL Data and Products*. http://www.wcc.nrcs.usda.gov/snow/

Natural Resources Conservation Service (NRCS). (2022b). *Web Soil Survey.* https://websoilsurvey.nrcs.usda.gov/app/WebSoilSurvey.aspx

Neary, D. G., Klopatek, C. C., DeBano, L. F., & Ffolliott, P. F. (1999). Fire effects on belowground sustainability: A review and synthesis. *Forest Ecology and Management*, *122*(1–2), 51–71. https://doi.org/10.1016/S0378-1127(99)00032-8

Nepal, S., Khatiwada, K. R., Pradhananga, S., Kralisch, S. (2020). Application of the J2000 Hydrological Model in the Panjshir catchment of the Hindu Kush Himalayan Region, Training Manual. International Centre for Integrated Mountain Development (ICIMOD), Kathmandu, Nepal.

Niemeyer, R. J., Bladon, K. D., & Woodsmith, R. D. (2020). Long-term hydrologic recovery after wildfire and post-fire forest management in the interior Pacific Northwest. *Hydrological Processes*, *34*(5), 1182–1197. https://doi.org/10.1002/hyp.13665

Nilsen, T. H. (1981). General Geology of the Northern Santa Lucia Range, California. *U.S. Geological Survey.*

Nolan, R. H., Lane, P. N. J., Benyon, R. G., Bradstock, R. A., & Mitchell, P. J. (2014). Changes in evapotranspiration following wildfire in resprouting eucalypt forests. *Ecohydrology*, 7,1363-1377. https://doi.org/10.1002/eco.1463

Nyman, P., Sheridan, G. J., Smith, H. G., & Lane, P. N. J. (2014). Modeling the effects of surface storage, macropore flow and water repellency on infiltration after wildfire. *Journal of Hydrology*, *513*, 301–313. https://doi.org/10.1016/j.jhydrol.2014.02.044

Nyman, P., Sheridan, G., & Lane, P. N. J. (2010). Synergistic effects of water repellency and macropore flow on the hydraulic conductivity of a burned forest soil, south-east Australia. *Hydrological Processes*, *24*(20), 2871–2887. https://doi.org/10.1002/hyp.7701

Onda, Y., Dietrich, W. E., & Booker, F. (2008). Evolution of overland flow after a severe forest fire, Point Reyes, California. *CATENA*, *72*(1), 13–20. https://doi.org/10.1016/j.catena.2007.02.003

Paço, T. A., David, T. S., Henriques, M. O., Pereira, J. S., Valente, F., Banza, J., Pereira, F. L., Pinto, C., & David, J. S. (2009). Evapotranspiration from a Mediterranean evergreen oak savannah: The role of trees and pasture. *Journal of Hydrology*, *369*(1–2), 98–106. https://doi.org/10.1016/j.jhydrol.2009.02.011

Poon, P. K., & Kinoshita, A. M. (2018). Spatial and temporal evapotranspiration trends after wildfire in semi-arid landscapes. *Journal of Hydrology*, *559*, 71–83. https://doi.org/10.1016/j.jhydrol.2018.02.023

PRISM Climate Group. (2022). *Time Series Values for Individual Locations*. https://prism.oregonstate.edu/explorer/

Schlesinger, W. H., & Jasechko, S. (2014). Transpiration in the global water cycle. *Agricultural and Forest Meteorology*, *189–190*, 115–117. https://doi.org/10.1016/j.agrformet.2014.01.011

Shuai, P., Chen, X., Mital, U., Coon, E. T., & Dwivedi, D. (2022). The effects of spatial and temporal resolution of gridded meteorological forcing on watershed hydrological responses. *Hydrology and Earth System Sciences*, *26*(8), 2245–2276. https://doi.org/10.5194/hess-26-2245-2022

Thornton, P. E., Shrestha, R., Thornton, M., Kao, S.-C., Wei, Y., & Wilson, B. E. (2021). Gridded daily weather data for North America with comprehensive uncertainty quantification. *Scientific Data*, *8*(1), 190. https://doi.org/10.1038/s41597-021-00973-0

Ukasha, M., Ramirez, J. A., & Niemann, J. D. (2022). Temporal Variations of NDVI and LAI and Interactions With Hydroclimatic Variables in a Large and Agro-Ecologically Diverse Region. *Journal of Geophysical Research: Biogeosciences*, *127*(4). https://doi.org/10.1029/2021JG006395

US Geological Survey (USGS). (2022a). *National Land Cover Database*. https://www.usgs.gov/centers/eros/science/national-land-cover-database

US Geological Survey (USGS). (2022b). *LCMAP Product Mosaic Downloads*. https://eros.usgs.gov/lcmap/apps/data-downloads

US Geological Survey (USGS). (2022c). *National Water Dashboard*. https://dashboard.waterdata.usgs.gov/app/nwd/en/?region=lower48&aoi=default

Veatch, W., Brooks, P. D., Gustafson, J. R., & Molotch, N. P. (2009). 'Quantifying the effects of forest canopy cover on net snow accumulation at a continental, mid-latitude site.' *Ecohydrology*, *2*(2), 115–128. https://doi.org/10.1002/eco.45

Veettil, A.V., Green, T.R., Kipka, H., Arabi, M., Lighthart, N., Mankin, K.R., & Clary, J. (2021). Fully distributed versus semi-distributed process simulation of a highly managed watershed with mixed land use and irrigation return flow. *Environmental Modelling and Software, 40*, 105000. https://doi.org/10.1016/j.envsoft.2021.105000.

Wagenbrenner, J. W., Ebel, B. A., Bladon, K. D., & Kinoshita, A. M. (2021). Post-wildfire hydrologic recovery in Mediterranean climates: A systematic review and case study to identify current knowledge and opportunities. *Journal of Hydrology*, *602*(126772), 1-16. https://doi.org/10.1016/j.jhydrol.2021.126772

Wells, R. (2023). Estimating Changes in Streamflow Attributable to Wildfire in Multiple Watersheds Using a Distributed Watershed Model. In press.

Westerling, A. L. (2016). Increasing western US forest wildfire activity: Sensitivity to changes in the timing of spring. *Philosophical Transactions of the Royal Society B: Biological Sciences*, *371*(1696), 1-10. https://doi.org/10.1098/rstb.2015.0178

Williams, A. P., Abatzoglou, J. T., Gershunov, A., Guzman-Morales, J., Bishop, D. A., Balch, J. K., & Lettenmaier, D. P. (2019a). Observed Impacts of Anthropogenic Climate Change on Wildfire in California. *Earth's Future*, *7*(8), 892–910. https://doi.org/10.1029/2019EF001210

Williams, A. P., Livneh, B., McKinnon, K. A., Hansen, W. D., Mankin, J. S., Cook, B. I., Smerdon, J. E., Varuolo-Clarke, A. M., Bjarke, N. R., Juang, C. S., & Lettenmaier, D. P. (2022). Growing impact of wildfire on western US water supply. *Proceedings of the National Academy of Sciences*, *119*(10), e2114069119. https://doi.org/10.1073/pnas.2114069119

Williams, C. H. S., Silins, U., Spencer, S. A., Wagner, M. J., Stone, M., & Emelko, M. B. (2019b). Net precipitation in burned and unburned subalpine forest stands after wildfire in the northern Rocky Mountains. *International Journal of Wildland Fire*, *28*(10), 750. https://doi.org/10.1071/WF18181

Zimmer, M. A., Kaiser, K. E., Blaszczak, J. R., Zipper, S. C., Hammond, J. C., Fritz, K. M., Costigan, K. H., Hosen, J., Godsey, S. E., Allen, G. H., Kampf, S., Burrows, R. M., Krabbenhoft, C. A., Dodds, W., Hale, R., Olden, J. D., Shanafield, M., DelVecchia, A. G., Ward, A. S., … Allen, D. C. (2020). Zero or not? Causes and consequences of zero-flow stream gage readings. *WIREs Water*, *7*(3), e1436. https://doi.org/10.1002/wat2.1436

# APPENDIX A

## FIRE HISTORY OF STUDY WATERSHEDS

Table A.1: Watershed fire history (NIFC, 2022). Asterisk denotes fire of interest.

| Watershed | Fire Name | Fire Year | Percent Burned |
|---|---|---|---|
| N. Eagle Creek | Ski Run | 2003 | 6.6 % |
| N. Eagle Creek | Little Bear* | 2012 | 100.0% |
| Lopez Creek | Gay | 1981 | 1.8% |
| Lopez Creek | Morretti | 1984 | 0.2% |
| Lopez Creek | Las Pilitas* | 1985 | 100.0% |
| Lopez Creek | Highway 41 | 1994 | 0.5% |
| Lopez Creek | Lopez | 2005 | 0.1% |
| Lopez Creek | Lopez | 2008 | 0.1% |
| Devil Canyon Creek | Panorama | 1954 | 89.8% |
| Devil Canyon Creek | Unnamed | 1970 | 0.8% |
| Devil Canyon Creek | Panorama | 1980 | 26.6% |
| Devil Canyon Creek | Jackson | 2001 | 0.3% |
| Devil Canyon Creek | Devil Canyon | 2001 | 1.6% |
| Devil Canyon Creek | Old* | 2003 | 95.7% |
| Devil Canyon Creek | Highway 18 | 2012 | 0.2% |
| E. Twin Creek | Arrowhead Springs | 1953 | 54.8% |
| E. Twin Creek | Unnamed | 1954 | 1.3% |
| E. Twin Creek | East Highland | 1956 | 0.0% |
| E. Twin Creek | Unnamed | 1957 | 3.6% |
| E. Twin Creek | Unnamed | 1970 | 4.0% |
| E. Twin Creek | Unnamed | 1972 | 1.8% |
| E. Twin Creek | Unnamed | 1974 | 1.5% |
| E. Twin Creek | Unnamed | 1975 | 5.2% |
| E. Twin Creek | Daley | 1979 | 3.9% |
| E. Twin Creek | Panorama | 1980 | 82.8% |
| E. Twin Creek | Highway 18 | 1994 | 0.2% |
| E. Twin Creek | Hemlock | 1997 | 0.0% |
| E. Twin Creek | Cold | 2002 | 0.1% |
| E. Twin Creek | Arrowhead* | 2002 | 43.2% |
| E. Twin Creek | Old* | 2003 | 95.2% |
| E. Twin Creek | Mile | 2017 | 0.1% |
| City Creek | City Creek | 1955 | 1.9% |
| City Creek | East Highland | 1956 | 20.5% |
| City Creek | McKinley | 1956 | 60.1% |
| City Creek | McKinley | 1960 | 0.0% |
| City Creek | Unnamed | 1968 | 0.1% |
| City Creek | Bear | 1970 | 28.2% |
| City Creek | Unnamed | 1973 | 0.1% |
| City Creek | Shadow | 1979 | 6.7% |

| | | | |
|---|---|---|---|
| City Creek | Unnamed | 1980 | 0.2% |
| City Creek | Panorama | 1980 | 3.9% |
| City Creek | Sycamore | 1980 | 13.5% |
| City Creek | Unnamed | 1985 | 1.1% |
| City Creek | Unnamed | 1989 | 0.0% |
| City Creek | Unnamed | 1991 | 2.2% |
| City Creek | Unnamed | 1992 | 2.2% |
| City Creek | Unnamed | 1993 | 1.4% |
| City Creek | Midnight | 1995 | 0.4% |
| City Creek | Rail | 1995 | 0.1% |
| City Creek | Roadside | 1995 | 0.4% |
| City Creek | Hemlock | 1997 | 5.7% |
| City Creek | Mill | 1997 | 0.7% |
| City Creek | Arrowhead | 2002 | 0.2% |
| City Creek | Harrison | 2002 | 0.3% |
| City Creek | Bridge* | 2003 | 9.7% |
| City Creek | Old* | 2003 | 93.3% |
| City Creek | Slide | 2007 | 2.3% |
| City Creek | McKinley | 2009 | 0.1% |
| City Creek | Hidden | 2017 | 0.4% |
| City Creek | Mart | 2017 | 1.5% |
| City Creek | Adobe | 2020 | 0.1% |
| City Creek | Easton | 2020 | 0.4% |
| Plunge Creek | Smiley | 1955 | 9.8% |
| Plunge Creek | East Highland | 1956 | 43.9% |
| Plunge Creek | McKinley | 1956 | 0.3% |
| Plunge Creek | Bear | 1970 | 81.6% |
| Plunge Creek | Sycamore | 1980 | 1.8% |
| Plunge Creek | Unnamed | 1993 | 0.3% |
| Plunge Creek | Unnamed | 1994 | 0.2% |
| Plunge Creek | Mill | 1997 | 11.5% |
| Plunge Creek | Bridge | 2003 | 0.0% |
| Plunge Creek | Old* | 2003 | 50.0% |
| Plunge Creek | Plunge | 2006 | 4.4% |
| Plunge Creek | Slide | 2007 | 24.2% |
| Plunge Creek | Unnamed | 2008 | 0.1% |
| Plunge Creek | Dollar | 2017 | 0.3% |
| Plunge Creek | Creek | 2018 | 0.3% |
| Plunge Creek | Mount R | 2020 | 0.6% |

# APPENDIX B
## CALIBRATED PARAMETER VALUES

Table B.1: Calibrated parameter values for each watershed.

| Parameter | North Eagle Creek | Lopez Creek | Devil Canyon Creek | City Creek | East Twin Creek | Plunge Creek |
|---|---|---|---|---|---|---|
| initMPS (m3/m3) | 0.363 | 0.231 | 0.478 | 0.499 | 0.272 | 0.287 |
| initLPS (m3/m3) | 0.062 | 0.020 | 0.189 | 0.200 | 0.119 | 0.092 |
| baseTemp (°C) | 4.337 | 3.933 | 3.947 | 4.376 | 4.608 | 4.482 |
| t_factor (mm/°C) | 1.175 | 1.665 | 0.079 | 0.167 | 0.119 | 0.037 |
| r_factor (mm/°C) | 1.336 | 3.421 | 0.055 | 0.153 | 0.224 | 0.036 |
| g_factor (mm) | 2.007 | 1.243 | 1.532 | 0.967 | 0.643 | 1.425 |
| snowCritDens (g/cm3) | 0.642 | 0.771 | 0.353 | 0.459 | 0.654 | 0.249 |
| ccf_factor (unitless) | 0.566 | 0.300 | 0.223 | 0.341 | 0.294 | 0.255 |
| snow_trans (°C) | 1.478 | 2.234 | 1.279 | 0.218 | 1.225 | 1.170 |
| snow_trs (°C) | 1.674 | -0.066 | -0.048 | -0.095 | -0.334 | -0.639 |
| a_rain (mm) | 1.295 | 4.341 | 4.305 | 3.386 | 1.990 | 3.179 |
| a_snow (mm) | 1.400 | 2.261 | 0.000 | 0.182 | 3.936 | 0.032 |
| soilMaxDPS (mm) | 3.601 | 1.358 | 0.232 | 1.098 | 4.197 | 1.805 |
| soilPolRed (unitless) | 4.962 | 6.832 | 40.93 | 79.16 | 68.72 | 73.88 |
| soilMaxInfSummer (cm/d) | 112.9 | 87.87 | 370.4 | 390.5 | 72.49 | 62.49 |
| soilMaxInfWinter (cm/d) | 90.00 | 115.2 | 386.7 | 398.8 | 172.9 | 397.1 |
| soilMaxInfSnow (cm/d) | 0.010 | 94.23 | 44.03 | 41.58 | 326.9 | 274.3 |
| soilDistMPSLPS (unitless) | 7.868 | 0.119 | 4.404 | 0.100 | 0.138 | 0.105 |
| soilDiffMPSLPS (unitless) | 1.819 | 6.457 | 6.611 | 9.143 | 0.106 | 1.998 |
| soilOutLPS (unitless) | 4.372 | 3.831 | 1.994 | 3.681 | 2.493 | 3.766 |
| soilLatVertLPS (unitless) | 0.012 | 0.997 | 0.456 | 0.505 | 0.444 | 1.330 |
| soilMaxPerc (cm/d) | 2.818 | 4.036 | 1.000 | 1.000 | 1.000 | 3.614 |
| geoMaxPerc (cm/d) | 0.001 | 0.587 | 0.360 | 0.334 | 0.561 | 0.942 |
| kdiff_layer (unitless) | 13.49 | 67.45 | 54.37 | 53.30 | 74.58 | 30.50 |
| BetaW (unitless) | 23.49 | 14.18 | 1.007 | 1.985 | 3.854 | 7.004 |
| lagSurfaceRunoff (unitless) | 2.000 | 1.354 | 1.726 | 1.016 | 1.776 | 1.005 |
| lagInterflow (unitless) | 1.900 | 2.396 | 1.819 | 1.320 | 1.916 | 2.825 |
| initRG1 (m3/m3) | 0.089 | 0.100 | 0.035 | 0.094 | 0.058 | 0.069 |
| initRG2 (m3/m3) | 0.083 | 0.063 | 0.081 | 0.100 | 0.064 | 0.020 |
| gwRG1RG2dist (unitless) | 0.634 | 0.900 | 0.894 | 0.837 | 0.883 | 0.895 |

| | | | | | | |
|---|---|---|---|---|---|---|
| gwRG1Fact (unitless) | 18.37 | 3.714 | 1.136 | 2.139 | 1.062 | 6.606 |
| gwRG2Fact (unitless) | 26.78 | 10.21 | 1.039 | 1.246 | 2.239 | 69.85 |
| gwCapRise (unitless) | 0.934 | 0.158 | 0.000 | 0.035 | 0.128 | 0.516 |
| flowRouteTA (unitless) | 94.82 | 0.265 | 0.092 | 0.153 | 0.110 | 0.186 |
| snowFactorA (unitless) | 0.149 | 0.017 | 0.071 | 0.141 | 0.129 | 0.030 |
| snowFactorB (unitless) | 0.142 | 0.172 | 0.083 | 0.105 | 0.057 | 0.106 |
| snowFactorC (unitless) | 0.318 | 0.099 | 0.088 | 0.333 | 0.121 | 0.324 |
| snowDensConst (unitless) | 0.392 | 0.080 | 0.418 | 0.441 | 0.878 | 0.869 |
| RG1_max (mm) | 60.41 | 310.7 | 86.80 | 244.7 | 195.1 | 51.91 |
| RG2_max (mm) | 602.4 | 163.0 | 576.5 | 1399 | 819.6 | 822.0 |
| RG1_k (d) | 996.3 | 73.19 | 987.0 | 13.67 | 400.3 | 99.23 |
| RG2_k (d) | 405.4 | 948.3 | 80.41 | 314.2 | 1669 | 1162 |
| RG1_active (unitless) | 4.641 | 5.581 | 0.758 | 6.572 | 2.260 | 2.439 |
| Kf_geo (cm/d) | 3.347 | 105.8 | 32.67 | 123.1 | 4.208 | 10.87 |
| PHU (CID 8-Evergreen) (unitless) | 877.1 | 616.8 | 2999 | 1267 | 2123 | 875.8 |
| BIO_E (CID 8-Evergreen) [(kg/ha)/(MJ/m2)] | 34.24 | 20.09 | 26.37 | 23.92 | 23.81 | 46.59 |
| BLAI (CID 8-Evergreen) (m2/m2) | 5.792 | 4.341 | 0.104 | 0.186 | 6.808 | 2.940 |
| FRGRW1 (CID 8-Evergreen) (unitless) | 0.016 | 0.010 | 0.277 | 0.223 | 0.328 | 0.330 |
| LAIMX1 (CID 8-Evergreen) (m2/m2) | 0.541 | 0.598 | 0.034 | 0.256 | 0.243 | 0.155 |
| FRGRW2 (CID 8-Evergreen) (unitless) | 0.557 | 0.400 | 0.500 | 0.543 | 0.469 | 0.558 |
| LAIMX2 (CID 8-Evergreen) (m2/m2) | 0.785 | 0.605 | 0.804 | 0.704 | 0.878 | 0.802 |
| PHU (CID 16-Brush) (unitless) | -- | 1417 | 2999 | 1725 | 1676 | 1992 |
| BIO_E (CID 16-Brush) [(kg/ha)/(MJ/m2)] | -- | 26.64 | 17.41 | 23.79 | 14.48 | 15.91 |
| BLAI (CID 16-Brush) (m2/m2) | -- | 2.249 | 0.102 | 4.119 | 4.066 | 6.695 |
| FRGRW1 (CID 16-Brush) (unitless) | -- | 0.392 | 0.285 | 0.215 | 0.194 | 0.261 |
| LAIMX1 (CID 16-Brush) (m2/m2) | -- | 0.377 | 0.020 | 0.251 | 0.409 | 0.350 |
| FRGRW2 (CID 16-Brush) (unitless) | -- | 0.436 | 0.500 | 0.493 | 0.517 | 0.596 |

| | | | | | | |
|---|---|---|---|---|---|---|
| LAIMX2 (CID 16-Brush) (m2/m2) | -- | 0.953 | 0.855 | 0.735 | 0.851 | 0.877 |

Table B.2: Calibrated soil parameter values for each watershed.

| **Watershed** | **SID** | **depth** (cm) | **aircapacity** ($m^3/m^3$) | **fieldcapacity** ($m^3/m^3$) | **deadcapacity** ($m^3/m^3$) | **Kf** (cm/d) | **root** (unitless) |
|---|---|---|---|---|---|---|---|
| **North** | 101 | 2.500 | 0.469 | 0.301 | 0.054 | 1.998 | 1 |
| **Eagle** | 102 | 7.500 | 0.494 | 0.327 | 0.027 | 59.27 | 1 |
| **Creek** | 103 | 30.00 | 0.495 | 0.191 | 0.060 | 68.77 | 1 |
| | 104 | 36.00 | 0.416 | 0.217 | 0.072 | 57.11 | 1 |
| **Lopez** | 101 | 27.00 | 0.381 | 0.359 | 0.011 | 104.9 | 1 |
| **Creek** | 102 | 13.00 | 0.540 | 0.143 | 0.055 | 139.9 | 1 |
| | 103 | 12.35 | 0.515 | 0.254 | 0.091 | 82.10 | 1 |
| | 104 | 44.70 | 0.548 | 0.142 | 0.059 | 135.7 | 1 |
| | 201 | 12.00 | 0.381 | 0.360 | 0.029 | 93.98 | 1 |
| | 202 | 189.3 | 0.544 | 0.146 | 0.015 | 123.7 | 1 |
| | 203 | 20.14 | 0.536 | 0.152 | 0.041 | 93.67 | 0 |
| **Devil** | 101 | 7.000 | 0.366 | 0.141 | 0.100 | 1.944 | 1 |
| **Canyon** | 102 | 79.95 | 0.550 | 0.141 | 0.012 | 365.0 | 1 |
| **Creek** | 103 | 79.66 | 0.550 | 0.149 | 0.011 | 47.13 | 0 |
| | 201 | 8.000 | 0.500 | 0.358 | 0.020 | 0.101 | 1 |
| | 202 | 59.97 | 0.550 | 0.348 | 0.011 | 386.8 | 1 |
| | 203 | 10.00 | 0.549 | 0.142 | 0.021 | 257.3 | 0 |
| | 501 | 16.00 | 0.423 | 0.140 | 0.099 | 1.940 | 1 |
| | 502 | 33.00 | 0.459 | 0.336 | 0.052 | 270.1 | 1 |
| | 503 | 59.95 | 0.549 | 0.207 | 0.010 | 318.2 | 1 |
| | 504 | 10.00 | 0.543 | 0.141 | 0.011 | 164.7 | 0 |
| | 601 | 11.00 | 0.361 | 0.265 | 0.099 | 0.104 | 1 |
| | 602 | 59.97 | 0.550 | 0.141 | 0.023 | 349.9 | 1 |
| | 603 | 22.00 | 0.549 | 0.146 | 0.011 | 168.5 | 0 |
| **City** | 101 | 7.000 | 0.382 | 0.141 | 0.100 | 0.273 | 1 |
| **Creek** | 102 | 79.95 | 0.550 | 0.239 | 0.014 | 352.7 | 1 |
| | 103 | 79.37 | 0.544 | 0.226 | 0.015 | 365.5 | 0 |
| | 201 | 8.000 | 0.400 | 0.345 | 0.023 | 1.947 | 1 |
| | 202 | 64.61 | 0.437 | 0.338 | 0.026 | 166.7 | 1 |
| | 203 | 10.00 | 0.467 | 0.206 | 0.068 | 198.3 | 0 |
| | 301 | 22.00 | 0.527 | 0.134 | 0.063 | 1.907 | 1 |
| | 302 | 24.00 | 0.511 | 0.316 | 0.038 | 90.84 | 1 |
| | 303 | 15.00 | 0.469 | 0.208 | 0.048 | 94.78 | 1 |
| | 304 | 91.14 | 0.503 | 0.238 | 0.052 | 75.38 | 0 |
| | 401 | 6.000 | 0.396 | 0.120 | 0.100 | 1.093 | 1 |
| | 402 | 16.77 | 0.384 | 0.125 | 0.099 | 38.88 | 1 |
| | 403 | 10.00 | 0.440 | 0.120 | 0.100 | 378.5 | 1 |
| **East** | 101 | 7.000 | 0.425 | 0.149 | 0.079 | 1.387 | 1 |
| **Twin** | 102 | 66.38 | 0.516 | 0.259 | 0.043 | 189.9 | 1 |
| **Creek** | 103 | 65.78 | 0.521 | 0.208 | 0.042 | 283.9 | 1 |
| | 104 | 55.09 | 0.451 | 0.183 | 0.053 | 263.5 | 0 |
| | 201 | 8.000 | 0.427 | 0.203 | 0.091 | 1.317 | 1 |
| | 202 | 49.30 | 0.531 | 0.357 | 0.013 | 141.9 | 1 |
| | 203 | 10.00 | 0.545 | 0.309 | 0.015 | 132.4 | 1 |
| | 204 | 25.71 | 0.544 | 0.165 | 0.016 | 276.9 | 0 |
| | 301 | 22.00 | 0.425 | 0.163 | 0.059 | 1.426 | 1 |
| | 302 | 24.00 | 0.454 | 0.292 | 0.049 | 131.7 | 1 |
| | 303 | 15.00 | 0.531 | 0.132 | 0.044 | 89.63 | 1 |
| | 304 | 81.75 | 0.405 | 0.316 | 0.086 | 90.31 | 0 |
| **Plunge** | 101 | 7.000 | 0.381 | 0.263 | 0.100 | 1.870 | 1 |
| **Creek** | 102 | 98.42 | 0.546 | 0.144 | 0.015 | 172.4 | 1 |
| | 103 | 98.89 | 0.549 | 0.146 | 0.071 | 300.8 | 0 |
| | 201 | 8.000 | 0.387 | 0.123 | 0.095 | 1.823 | 1 |
| | 202 | 32.40 | 0.541 | 0.120 | 0.099 | 184.5 | 1 |

| | | | | | | |
|---|---|---|---|---|---|---|
| 203 | 10.00 | 0.524 | 0.241 | 0.064 | 173.4 | 0 |
| 301 | 22.00 | 0.442 | 0.359 | 0.011 | 0.602 | 1 |
| 302 | 24.00 | 0.548 | 0.182 | 0.013 | 194.2 | 1 |
| 303 | 15.00 | 0.462 | 0.216 | 0.029 | 92.6 | 1 |
| 304 | 74.70 | 0.405 | 0.350 | 0.042 | 168.2 | 0 |
| 401 | 6.000 | 0.385 | 0.121 | 0.099 | 0.853 | 1 |
| 402 | 22.06 | 0.546 | 0.255 | 0.011 | 148.1 | 1 |
| 403 | 10.00 | 0.534 | 0.134 | 0.091 | 366.6 | 1 |

# APPENDIX C
## CALIBRATION SCHEME FOR DEVIL CANYON CREEK

```
calibration_start "1994-10-01"         // calibration start date  (change for prefire)

start_month_of_year 1

rounds 5                               // calibration rounds, default 1

//model_stdout false

summary_file "lucaNS_data.txt"

trace_file "trace_of_NS.txt"


// step definitions



step(1){          //initial storages

max_exec(20)

of_percentage(0.1)

parameter {

        initMPS(lower:0.1, upper:0.5, calib_strategy:INDIVIDUAL) // initial value used for middle pore storage (MPS) compartment

        initLPS(lower:0.0, upper:0.2, calib_strategy:INDIVIDUAL) // initial value used for lower pore storage (LPS) compartment originally 0.5 max

        initRG1(lower:0.01, upper:0.1, calib_strategy:INDIVIDUAL) // Relative filling of the upper groundwater storage at beginning of the simulation, 1=filled to capacity, 0=empty originally 0.5 max

        initRG2(lower:0.01, upper:0.1, calib_strategy:INDIVIDUAL) // Relative filling of the lower groundwater storage at beginning of the simulation, 1=filled to capacity, 0=empty originally 0.5 max

}

objfunc(method:NSLOG, timestep:DAILY, weight: 0.6) {

        simulated(file:"Outlet.csv", table:"output", column:"catchmentSimRunoff")
```

```
        observed(file:"$data/orun_Devils_Canyon_Creek_nozeroflow.csv",
table:"observed",column:"orun[1]")
}
objfunc(method:NS, timestep:DAILY, weight: 0.2) {
        simulated(file:"Outlet.csv", table:"output", column:"catchmentSimRunoff")
        observed(file:"$data/orun_Devils_Canyon_Creek_nozeroflow.csv",
table:"observed",column:"orun[1]")
}
objfunc(method:KGE, timestep:DAILY, weight: 0.2) {
        simulated(file:"Outlet.csv", table:"output", column:"catchmentSimRunoff")
        observed(file:"$data/orun_Devils_Canyon_Creek_nozeroflow.csv",
table:"observed",column:"orun[1]")
}
}

step(2) { //baseflow
max_exec(3000)
of_percentage(0.1)
parameter {
        RG1_max(lower:50, upper:350, calib_strategy:INDIVIDUAL)
        RG2_max(lower:500, upper:1000, calib_strategy:INDIVIDUAL)
        RG1_k(lower:500, upper:1200, calib_strategy:INDIVIDUAL)
        RG2_k(lower:50, upper:2000, calib_strategy:INDIVIDUAL)
        RG1_active(lower:0.2, upper:4, calib_strategy:INDIVIDUAL)
        Kf_geo(lower:5, upper:100, calib_strategy:INDIVIDUAL)
}
objfunc(method:NS, timestep:DAILY, weight: 0.3) {
        simulated(file:"Outlet.csv", table:"output", column:"catchmentSimRunoff")
        observed(file:"$data/orun_Devils_Canyon_Creek_nozeroflow.csv",
table:"observed",column:"orun[1]")
```

```
}
objfunc(method:NSLOG, timestep:DAILY, weight: 0.4) {
        simulated(file:"Outlet.csv", table:"output", column:"catchmentSimRunoff")
        observed(file:"$data/orun_Devils_Canyon_Creek_nozeroflow.csv",
table:"observed",column:"orun[1]")
}
objfunc(method:KGE, timestep:DAILY, weight: 0.3) {
        simulated(file:"Outlet.csv", table:"output", column:"catchmentSimRunoff")
        observed(file:"$data/orun_Devils_Canyon_Creek_nozeroflow.csv",
table:"observed",column:"orun[1]")
}
}


step(3){        //plant param
max_exec(3000)
of_percentage(0.1)
parameter {
        PHU(lower:600, upper:3000, calib_strategy:INDIVIDUAL,filter_param:"crop\$CID",
subset:"8,16") //shrub
        BLAI(lower:0.1, upper:10, calib_strategy:INDIVIDUAL,filter_param:"crop\$CID",
subset:"8,16") //shrub
        BIO_E(lower:1, upper:50, calib_strategy:INDIVIDUAL,filter_param:"crop\$CID",
subset:"8,16") //shrub
        FRGRW1(lower:0.01, upper:0.3,
calib_strategy:INDIVIDUAL,filter_param:"crop\$CID", subset:"8,16") //shrub
        LAIMX1(lower:0.01, upper:0.1, calib_strategy:INDIVIDUAL,filter_param:"crop\$CID",
subset:"8,16") //shrub
        LAIMX2(lower:0.8, upper:0.99, calib_strategy:INDIVIDUAL,filter_param:"crop\$CID",
subset:"8,16") //shrubshrub
}
objfunc(method:NS, timestep:DAILY, weight: 0.4) {
```

```
        simulated(file:"Outlet.csv", table:"output", column:"catchmentSimRunoff")

        observed(file:"$data/orun_Devils_Canyon_Creek_nozeroflow.csv",
table:"observed",column:"orun[1]")

}

objfunc(method:NSLOG, timestep:DAILY, weight: 0.3) {

        simulated(file:"Outlet.csv", table:"output", column:"catchmentSimRunoff")

        observed(file:"$data/orun_Devils_Canyon_Creek_nozeroflow.csv",
table:"observed",column:"orun[1]")

}

objfunc(method:KGE, timestep:DAILY, weight: 0.3) {

        simulated(file:"Outlet.csv", table:"output", column:"catchmentSimRunoff")

        observed(file:"$data/orun_Devils_Canyon_Creek_nozeroflow.csv",
table:"observed",column:"orun[1]")

}

}


step(4){        //evapotranpiration

max_exec(3000)

of_percentage(0.1)

parameter {

        BetaW(lower:1, upper:40, calib_strategy:INDIVIDUAL) // Coefficient used to calculate
transpiration in soil layers, no range given

        soilPolRed(lower:0.1, upper:80, calib_strategy:INDIVIDUAL) // Polynomial reduction
factor for reduction of potential evaporation with limited water supply, unitless

}

objfunc(method:NS, timestep:DAILY, weight: 0.4) {

        simulated(file:"Outlet.csv", table:"output", column:"catchmentSimRunoff")

        observed(file:"$data/orun_Devils_Canyon_Creek_nozeroflow.csv",
table:"observed",column:"orun[1]")

}
```

```
objfunc(method:NSLOG, timestep:DAILY, weight: 0.3) {
        simulated(file:"Outlet.csv", table:"output", column:"catchmentSimRunoff")
        observed(file:"$data/orun_Devils_Canyon_Creek_nozeroflow.csv",
table:"observed",column:"orun[1]")
}
objfunc(method:KGE, timestep:DAILY, weight: 0.3) {
        simulated(file:"Outlet.csv", table:"output", column:"catchmentSimRunoff")
        observed(file:"$data/orun_Devils_Canyon_Creek_nozeroflow.csv",
table:"observed",column:"orun[1]")
}
}

step(5){        //interception
max_exec(3000)
of_percentage(0.1)
parameter {
        a_rain(lower:0, upper:5, calib_strategy:INDIVIDUAL) // Maximum storage capacity per
Leaf Area Index (LAI) for rain, mm *changed upper from 1 to 1.5
        a_snow(lower:0, upper:5, calib_strategy:INDIVIDUAL) // Maximum storage capacity
per LAI for snow
}
objfunc(method:NS, timestep:DAILY, weight: 0.4) {
        simulated(file:"Outlet.csv", table:"output", column:"catchmentSimRunoff")
        observed(file:"$data/orun_Devils_Canyon_Creek_nozeroflow.csv",
table:"observed",column:"orun[1]")
}
objfunc(method:NSLOG, timestep:DAILY, weight: 0.3) {
        simulated(file:"Outlet.csv", table:"output", column:"catchmentSimRunoff")
        observed(file:"$data/orun_Devils_Canyon_Creek_nozeroflow.csv",
table:"observed",column:"orun[1]")
```

```
}
objfunc(method:KGE, timestep:DAILY, weight: 0.3) {
        simulated(file:"Outlet.csv", table:"output", column:"catchmentSimRunoff")
        observed(file:"$data/orun_Devils_Canyon_Creek_nozeroflow.csv",
table:"observed",column:"orun[1]")
}
}


step(6){     //snow
max_exec(5000)
of_percentage(0.1)
parameter {
        baseTemp(lower:0, upper:5, calib_strategy:INDIVIDUAL) // base melting temperature
for snow
        t_factor(lower:0, upper:5, calib_strategy:INDIVIDUAL) // Temperature factor for snow
melt calculation
        r_factor(lower:0, upper:5, calib_strategy:INDIVIDUAL) // Rain factor for snow melt
calculation
        g_factor(lower:0, upper:5, calib_strategy:INDIVIDUAL) // Soil heat factor for snow melt
calculation
        snowCritDens(lower:0.2, upper:0.8,calib_strategy:INDIVIDUAL) // Snowpack density
beyond which free water is released
        snow_trans(lower:0, upper:2.5, calib_strategy:INDIVIDUAL)
        snow_trs(lower:-5, upper:0, calib_strategy:INDIVIDUAL)
        ccf_factor(lower:0.0001, upper:0.5, calib_strategy:INDIVIDUAL) // Cold content factor
        //snowFactorA(lower:0.0001, upper:0.2, calib_strategy:INDIVIDUAL)
        //snowFactorB(lower:0.0001, upper:0.2, calib_strategy:INDIVIDUAL)
        //snowFactorC(lower:0.0001, upper:0.5, calib_strategy:INDIVIDUAL)
        //snowDensConst(lower:0.01, upper:1, calib_strategy:INDIVIDUAL)
}
```

```
objfunc(method:NS, timestep:DAILY, weight: 0.4) {
        simulated(file:"Outlet.csv", table:"output", column:"catchmentSimRunoff")
        observed(file:"$data/orun_Devils_Canyon_Creek_nozeroflow.csv",
table:"observed",column:"orun[1]")
}
objfunc(method:NSLOG, timestep:DAILY, weight: 0.3) {
        simulated(file:"Outlet.csv", table:"output", column:"catchmentSimRunoff")
        observed(file:"$data/orun_Devils_Canyon_Creek_nozeroflow.csv",
table:"observed",column:"orun[1]")
}
objfunc(method:KGE, timestep:DAILY, weight: 0.3) {
        simulated(file:"Outlet.csv", table:"output", column:"catchmentSimRunoff")
        observed(file:"$data/orun_Devils_Canyon_Creek_nozeroflow.csv",
table:"observed",column:"orun[1]")
}
}

step(7){ //soil zone and percolation
max_exec(15000)
of_percentage(0.1)
parameter {
        soilMaxInfSummer(lower:0.1, upper:400, calib_strategy:INDIVIDUAL) // Coefficient
used to calculate maximum infiltration in summer, cm/d 2
        soilMaxInfWinter(lower:0.1, upper:400, calib_strategy:INDIVIDUAL) // Coefficient
used to calculate maximum infiltration in winter, cm/d 2
        soilMaxInfSnow(lower:0.1, upper:400, calib_strategy:INDIVIDUAL) // Coefficient used
to calculate maximum infiltration for snow covered areas, cm/d 2
        soilDistMPSLPS(lower:0.1, upper:10, calib_strategy:INDIVIDUAL) // Coefficient for
distribution of infiltration to the LPS and MPS soil storages, cm/d 10
        soilMaxDPS(lower:0, upper:5, calib_strategy:INDIVIDUAL) // Maximum depression
storage capacity, mm
```

kf(lower:0.1, upper:2, calib_strategy:INDIVIDUAL, filter_param:"soils\$SID", subset:"101,201,501,601") // Maximum saturated hydraulic conductivity (cm/d), range: 1 to 9999
2

}

objfunc(method:NS, timestep:DAILY, weight: 0.4) {

simulated(file:"Outlet.csv", table:"output", column:"catchmentSimRunoff")

observed(file:"$data/orun_Devils_Canyon_Creek_nozeroflow.csv", table:"observed",column:"orun[1]")

}

objfunc(method:NSLOG, timestep:DAILY, weight: 0.3) {

simulated(file:"Outlet.csv", table:"output", column:"catchmentSimRunoff")

observed(file:"$data/orun_Devils_Canyon_Creek_nozeroflow.csv", table:"observed",column:"orun[1]")

}

objfunc(method:KGE, timestep:DAILY, weight: 0.3) {

simulated(file:"Outlet.csv", table:"output", column:"catchmentSimRunoff")

observed(file:"$data/orun_Devils_Canyon_Creek_nozeroflow.csv", table:"observed",column:"orun[1]")

}

}

step(8){ //soil zone 1 (FLG)

max_exec(10000)

of_percentage(0.1)

parameter {

kf(lower:15, upper:400, calib_strategy:INDIVIDUAL, filter_param:"soils\$SID", subset:"102,103") // Maximum saturated hydraulic conductivity (cm/d), range: 1 to 9999

aircapacity(lower:0.36, upper:0.55, calib_strategy:INDIVIDUAL, filter_param:"soils\$SID", subset:"101,102,103") // Saturated soil water content, mm or vol., depending on initSWC, 1 to 9999

```
        deadcapacity(lower:0.01, upper:0.1, calib_strategy:INDIVIDUAL,
filter_param:"soils\$SID", subset:"101,102,103")

        fieldcapacity(lower:0.14, upper:0.36, calib_strategy:INDIVIDUAL,
filter_param:"soils\$SID", subset:"101,102,103") // 1/3 bar soil water content, amount of soil
moisture or water content held in the soil after excess water has drained away and the rate of
downward movement has decreased

        depth(lower:20, upper:80, calib_strategy:INDIVIDUAL, filter_param:"soils\$SID",
subset:"102,103") // soil depth

}

objfunc(method:NS, timestep:DAILY, weight: 0.4) {

        simulated(file:"Outlet.csv", table:"output", column:"catchmentSimRunoff")

        observed(file:"$data/orun_Devils_Canyon_Creek_nozeroflow.csv",
table:"observed",column:"orun[1]")

}

objfunc(method:NSLOG, timestep:DAILY, weight: 0.3) {

        simulated(file:"Outlet.csv", table:"output", column:"catchmentSimRunoff")

        observed(file:"$data/orun_Devils_Canyon_Creek_nozeroflow.csv",
table:"observed",column:"orun[1]")

}

objfunc(method:KGE, timestep:DAILY, weight: 0.3) {

        simulated(file:"Outlet.csv", table:"output", column:"catchmentSimRunoff")

        observed(file:"$data/orun_Devils_Canyon_Creek_nozeroflow.csv",
table:"observed",column:"orun[1]")

}

}


step(9){ //soil zone 2 (DNG)

max_exec(10000)

of_percentage(0.1)

parameter {
```

kf(lower:10, upper:400, calib_strategy:INDIVIDUAL, filter_param:"soils\$SID", subset:"202,203") // Maximum saturated hydraulic conductivity (cm/d), range: 1 to 9999

aircapacity(lower:0.36, upper:0.55, calib_strategy:INDIVIDUAL, filter_param:"soils\$SID", subset:"201,202,203") // Saturated soil water content, mm or vol., depending on initSWC, 1 to 9999

deadcapacity(lower:0.01, upper:0.1, calib_strategy:INDIVIDUAL, filter_param:"soils\$SID", subset:"201,202,203")

fieldcapacity(lower:0.14, upper:0.36, calib_strategy:INDIVIDUAL, filter_param:"soils\$SID", subset:"201,202,203") // 1/3 bar soil water content, amount of soil moisture or water content held in the soil after excess water has drained away and the rate of downward movement has decreased

depth(lower:20, upper:60, calib_strategy:INDIVIDUAL, filter_param:"soils\$SID", subset:"202") // soil depth

}

objfunc(method:NS, timestep:DAILY, weight: 0.4) {

simulated(file:"Outlet.csv", table:"output", column:"catchmentSimRunoff")

observed(file:"$data/orun_Devils_Canyon_Creek_nozeroflow.csv", table:"observed",column:"orun[1]")

}

objfunc(method:NSLOG, timestep:DAILY, weight: 0.3) {

simulated(file:"Outlet.csv", table:"output", column:"catchmentSimRunoff")

observed(file:"$data/orun_Devils_Canyon_Creek_nozeroflow.csv", table:"observed",column:"orun[1]")

}

objfunc(method:KGE, timestep:DAILY, weight: 0.3) {

simulated(file:"Outlet.csv", table:"output", column:"catchmentSimRunoff")

observed(file:"$data/orun_Devils_Canyon_Creek_nozeroflow.csv", table:"observed",column:"orun[1]")

}

}

step(10){ //soil zone 5 (CMF)

```
max_exec(10000)

of_percentage(0.1)

parameter {

        kf(lower:8, upper:400, calib_strategy:INDIVIDUAL, filter_param:"soils\$SID",
subset:"502,503,504") // Maximum saturated hydraulic conductivity (cm/d), range: 1 to 9999

        aircapacity(lower:0.36, upper:0.55, calib_strategy:INDIVIDUAL,
filter_param:"soils\$SID", subset:"501,502,503,504") // Saturated soil water content, mm or vol.,
depending on initSWC, 1 to 9999

        deadcapacity(lower:0.01, upper:0.1, calib_strategy:INDIVIDUAL,
filter_param:"soils\$SID", subset:"501,502,503,504")

        fieldcapacity(lower:0.14, upper:0.36, calib_strategy:INDIVIDUAL,
filter_param:"soils\$SID", subset:"501,502,503,504") // 1/3 bar soil water content, amount of soil
moisture or water content held in the soil after excess water has drained away and the rate of
downward movement has decreased

        depth(lower:20, upper:60, calib_strategy:INDIVIDUAL, filter_param:"soils\$SID",
subset:"503") // soil depth

}

objfunc(method:NS, timestep:DAILY, weight: 0.4) {

        simulated(file:"Outlet.csv", table:"output", column:"catchmentSimRunoff")

        observed(file:"$data/orun_Devils_Canyon_Creek_nozeroflow.csv",
table:"observed",column:"orun[1]")

}

objfunc(method:NSLOG, timestep:DAILY, weight: 0.3) {

        simulated(file:"Outlet.csv", table:"output", column:"catchmentSimRunoff")

        observed(file:"$data/orun_Devils_Canyon_Creek_nozeroflow.csv",
table:"observed",column:"orun[1]")

}

objfunc(method:KGE, timestep:DAILY, weight: 0.3) {

        simulated(file:"Outlet.csv", table:"output", column:"catchmentSimRunoff")

        observed(file:"$data/orun_Devils_Canyon_Creek_nozeroflow.csv",
table:"observed",column:"orun[1]")

}
```

```
}


step(11){ //soil zone 6 (Dag)

max_exec(10000)

of_percentage(0.1)

parameter {

        kf(lower:15, upper:400, calib_strategy:INDIVIDUAL, filter_param:"soils\$SID",
subset:"602,603") // Maximum saturated hydraulic conductivity (cm/d), range: 1 to 9999

        aircapacity(lower:0.36, upper:0.55, calib_strategy:INDIVIDUAL,
filter_param:"soils\$SID", subset:"601,602,603") // Saturated soil water content, mm or vol.,
depending on initSWC, 1 to 9999

        deadcapacity(lower:0.01, upper:0.1, calib_strategy:INDIVIDUAL,
filter_param:"soils\$SID", subset:"601,602,603")

        fieldcapacity(lower:0.14, upper:0.36, calib_strategy:INDIVIDUAL,
filter_param:"soils\$SID", subset:"601,602,603") // 1/3 bar soil water content, amount of soil
moisture or water content held in the soil after excess water has drained away and the rate of
downward movement has decreased

        depth(lower:20, upper:60, calib_strategy:INDIVIDUAL, filter_param:"soils\$SID",
subset:"602") // soil depth

}

objfunc(method:NS, timestep:DAILY, weight: 0.4) {

        simulated(file:"Outlet.csv", table:"output", column:"catchmentSimRunoff")

        observed(file:"$data/orun_Devils_Canyon_Creek_nozeroflow.csv",
table:"observed",column:"orun[1]")

}

objfunc(method:NSLOG, timestep:DAILY, weight: 0.3) {

        simulated(file:"Outlet.csv", table:"output", column:"catchmentSimRunoff")

        observed(file:"$data/orun_Devils_Canyon_Creek_nozeroflow.csv",
table:"observed",column:"orun[1]")

}

objfunc(method:KGE, timestep:DAILY, weight: 0.3) {

        simulated(file:"Outlet.csv", table:"output", column:"catchmentSimRunoff")
```

```
        observed(file:"$data/orun_Devils_Canyon_Creek_nozeroflow.csv",
table:"observed",column:"orun[1]")

}

}



step(12){

max_exec(20000)

of_percentage(0.1)

parameter {

        lagInterflow(lower:1, upper:2, calib_strategy:INDIVIDUAL)

        soilOutLPS(lower:0.1, upper:5, calib_strategy:INDIVIDUAL) // Coefficient for
definition of LPS outflow, unitless

        soilLatVertLPS(lower:0.01, upper:7, calib_strategy:INDIVIDUAL) // Coefficient for
distribution of the LPS outflow on the lateral (interflow) and vertical (percolation) component,
unitless *changed lower from 0.5 to 0.001

        kdiff_layer(lower:5, upper:80, calib_strategy:INDIVIDUAL) // Coefficient used to
calculate water flux between soil layers

        soilDiffMPSLPS(lower:0.1, upper:10, calib_strategy:INDIVIDUAL) // Coefficient for
the definition of the diffusion amount of the LPS storage in relation to MPS at the end of a time
s, unitless

        //soilMaxPerc(lower:1, upper:5, calib_strategy:INDIVIDUAL) // Maximum percolation
rate through a soil layer

        gwCapRise(lower:0, upper:1, calib_strategy:INDIVIDUAL) // Capillary rise coefficient

        gwRG1Fact(lower:1, upper:20, calib_strategy:INDIVIDUAL) // RG1 (shallow
groundwater storage) outflow coefficient

        gwRG2Fact(lower:1, upper:80, calib_strategy:INDIVIDUAL) // RG2 (deep groundwater
storage) outflow coefficient

        gwRG1RG2dist(lower:0.1, upper:0.9, calib_strategy:INDIVIDUAL) // RG1 to RG2
gradient (distribution) coefficient

        geoMaxPerc(lower:0, upper:1, calib_strategy:INDIVIDUAL) // Maximum percolation
rate to groundwater
```

```
}
objfunc(method:NS, timestep:DAILY, weight: 0.4) {
        simulated(file:"Outlet.csv", table:"output", column:"catchmentSimRunoff")
        observed(file:"$data/orun_Devils_Canyon_Creek_nozeroflow.csv",
table:"observed",column:"orun[1]")
}
objfunc(method:NSLOG, timestep:DAILY, weight: 0.3) {
        simulated(file:"Outlet.csv", table:"output", column:"catchmentSimRunoff")
        observed(file:"$data/orun_Devils_Canyon_Creek_nozeroflow.csv",
table:"observed",column:"orun[1]")
}
objfunc(method:KGE, timestep:DAILY, weight: 0.3) {
        simulated(file:"Outlet.csv", table:"output", column:"catchmentSimRunoff")
        observed(file:"$data/orun_Devils_Canyon_Creek_nozeroflow.csv",
table:"observed",column:"orun[1]")
}
}

step(13){ //Surface Runoff
max_exec(5000)
of_percentage(0.1)
parameter {
        flowRouteTA(lower:0.01, upper:1000, calib_strategy:INDIVIDUAL) // flood routing
coefficient
        lagSurfaceRunoff(lower:1, upper:2, calib_strategy:INDIVIDUAL)
        //Ksink(lower:0.01, upper:80, calib_strategy:INDIVIDUAL)
}
objfunc(method:NS, timestep:DAILY, weight: 0.4) {
        simulated(file:"Outlet.csv", table:"output", column:"catchmentSimRunoff")
```

```
        observed(file:"$data/orun_Devils_Canyon_Creek_nozeroflow.csv",
table:"observed",column:"orun[1]")

}

objfunc(method:NSLOG, timestep:DAILY, weight: 0.3) {

        simulated(file:"Outlet.csv", table:"output", column:"catchmentSimRunoff")

        observed(file:"$data/orun_Devils_Canyon_Creek_nozeroflow.csv",
table:"observed",column:"orun[1]")

}

objfunc(method:KGE, timestep:DAILY, weight: 0.3) {

        simulated(file:"Outlet.csv", table:"output", column:"catchmentSimRunoff")

        observed(file:"$data/orun_Devils_Canyon_Creek_nozeroflow.csv",
table:"observed",column:"orun[1]")

}

}
```